buildings

Article

Development of a Framework for Assessing Bitumen Fatigue Cracking Performance under Different Temperatures and Aging Conditions

Songtao Lv [1], Dongdong Ge [1], Shihao Cao [1], Dingyuan Liu [1], Wenhui Zhang [1], Cheng-Hui Li [2] and Milkos Borges Cabrera [1,*]

1 School of Traffic and Transportation Engineering, Changsha University of Science & Technology, Changsha 410114, China; lst@csust.edu.cn (S.L.); dge1@csust.edu.cn (D.G.); csh@stu.csust.edu.cn (S.C.); nf@stu.csust.edu.cn (D.L.); whzz@stu.csust.edu.cn (W.Z.)
2 State Key Laboratory of Coordination Chemistry, School of Chemistry and Chemical Engineering, Collaborative Innovation Center of Advanced Microstructures, Nanjing University, Nanjing 210093, China; chli@nju.edu.cn
* Correspondence: combigra2013@gmail.com

Abstract: A full understanding of bitumen fatigue cracking behavior is extremely important as this phenomenon has a considerable influence on bituminous pavement performance. The current framework for assessing this asphalt binder property is inconsistent in ranking bitumen fatigue performance in terms of the failure definition and damage characteristic curve (DCC) analysis. This study used four different types of asphalt binders: neat asphalt (NA), self-healing thermoplastic polyurethane (STP)-modified bitumen, self-healing poly (dimethyl siloxane) crosslinked with urea bond (IPA1w)-modified bitumen, and styrene–butadiene–styrene (SBS)-modified bitumen (SBSB). All the bitumens were subjected to short-term and long-term aging, and they were also tested by utilizing the linear amplitude sweep (LAS) test and the simplified viscoelastic continuum damage (S-VECD) model. LAS and S-VECD procedures were used to apply the newly proposed and current frameworks in order to analyze bitumen performance. The current framework showed that the bitumens that used a higher number of loading cycles (N) to reach their failure points (N_f) failed to exhibit greater fatigue performances in terms of DCC analysis. The developed framework (mainly based on the damage intensity [S] instead of N) was used to solve the inconsistency between the failure definition and DCC assessment in ranking bitumen performance. Additionally, the current framework (failure criterion) presented two R^2 values below 0.1, but the developed framework (failure criterion) showed that all R^2 values were greater than 0.9. The developed framework represents a turning point because, for the first time, this type of procedure is mainly being based on S instead of N. Although further tests are needed to confirm its efficiency, it eliminates the inconsistency between the failure definition and DCC assessment.

Keywords: failure definition; failure criterion; bitumen fatigue cracking performance; bitumen fatigue failure point

check for updates

Citation: Lv, S.; Ge, D.; Cao, S.; Liu, D.; Zhang, W.; Li, C.-H.; Borges Cabrera, M. Development of a Framework for Assessing Bitumen Fatigue Cracking Performance under Different Temperatures and Aging Conditions. *Buildings* **2024**, *14*, 311. https://doi.org/10.3390/buildings14020311

Academic Editors: Bjorn Birgisson and Ramadhansyah Putra Jaya

Received: 28 November 2023
Revised: 4 January 2024
Accepted: 15 January 2024
Published: 23 January 2024

Copyright: © 2024 by the authors. Licensee MDPI, Basel, Switzerland. This article is an open access article distributed under the terms and conditions of the Creative Commons Attribution (CC BY) license (https://creativecommons.org/licenses/by/4.0/).

1. Introduction

Bitumen fatigue cracking resistance is an important property that has a substantial effect on flexible pavement fatigue performance [1]. Fatigue cracking occurrence in asphalt concrete mostly initiates and proliferates through asphalt binder. Hence, the bitumen fatigue behavior is a key property for ensuring the superior fatigue performance of asphalt pavement [2–4].

Failure definition and the failure criterion are essential concepts for assessing bitumen fatigue cracking performance, and the LAS test and S-VECD model are utilized to define both of these parameters. The LAS test is an efficient and quick process that is explained in

AASHTO TP 101-14 [5,6], and it has shown high efficiency in illustrating bitumen fatigue behavior [7,8]. LAS test results should be interpreted by utilizing the S-VECD theory as this model has a proven high efficiency in processing LAS data, as well as in evaluating and predicting bitumen fatigue performance [9–11]. Afterward, by conducting the S-VECD procedure, the DCC can be obtained. This special curve represents the correlation between the material integrity (C) (also named pseudo-stiffness and the normalized dynamic shear modulus) and the damage intensity (S), which is an internal state variable that results from considering the damage evolution of Schapery's work potential theory. Its formulation is as follows [12,13]:

$$\frac{dS}{d\vartheta} = \left(-\frac{\partial W^R}{\partial S}\right)^{\alpha}, \tag{1}$$

where ϑ, W^R, and α are the reduced time, pseudo-strain energy, and damage evolution rate, respectively.

The failure definition establishes the bitumen fatigue life (N_f), which is the number of loading cycles it takes to reach the failure point and should be meticulously selected considering the experimental data and scientifically proven frameworks [14]. In asphalt pavements, identifying, predicting, and completely understanding bitumen fatigue life and cracking propagation represents a challenge for scholars [15,16]. As a result, numerous studies have been conducted to address this topic.

Safaei et al. [17] proved that the peak of the phase angle (δ) (in δ vs. N graph) was not a suitable failure definition for NA and warm mix asphalt (WMA) binders because its trend was unclear. However, this concept has been commonly used in asphalt mixtures [18–20]. Consequently, this study proposed a new failure definition at the C × N peak by analyzing numerous DCCs, δs, and dynamic shear moduli (G*). Figure 1 shows the fatigue failure definition at the C × N peak displayed in this mentioned study "Reprinted/adapted with permission from Ref. [17]. Copyright 2014, Taylor & Francis Group". Wang et al. [8] introduced a new failure definition at the τ (shear stress) × N peak based on the δ, τ, shear strain, pseudo-strain, as well as in the total, stored, and released pseudo-strain energy (PSE) value analyses. This research tested crumb rubber (CR) modified bitumen, SBSB, and NA. The researchers proved that the τ × N peak and maximum stored PSE were equivalent. Hence, this latter parameter could be considered a suitable failure definition for asphalt binder, which comprises energy [9]. Figure 2 illustrates the shear stress and phase angle tendencies that applied while conducting the LAS test [8] "Reprinted/adapted with permission from Ref. [8] Copyright 2015, Taylor & Francis Group ".

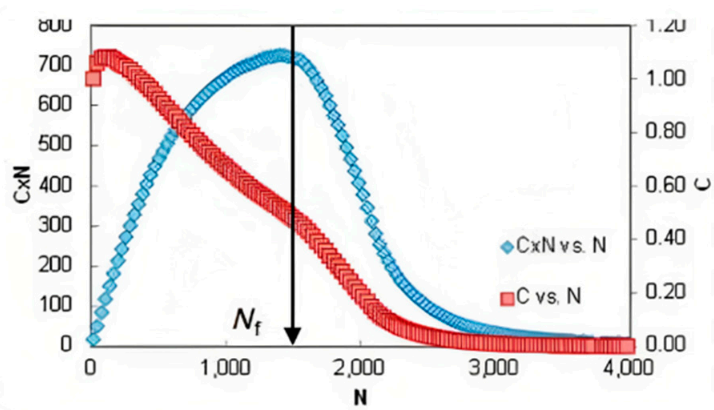

Figure 1. Fatigue failure definition of the asphalt binder at the C × N peak [17].

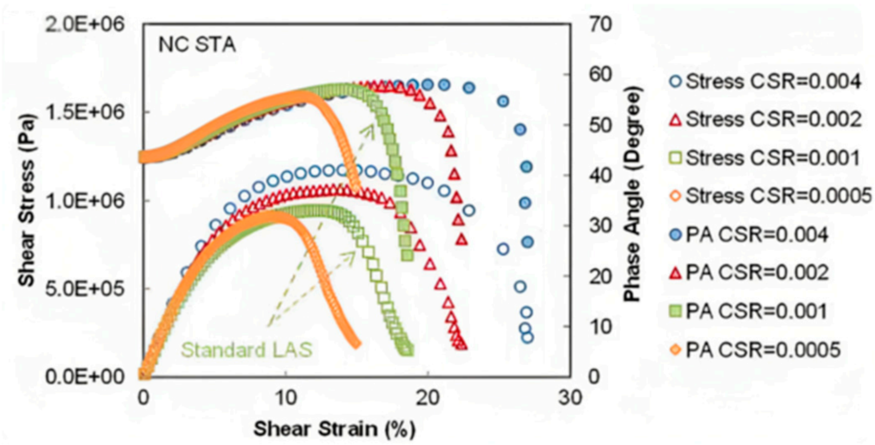

Figure 2. LAS test data from the different CSRs, phase angles, and shear stress evolutions [8].

Zhou et al. [21] found that some long-term aged bitumens exhibited higher N_f than unaged and short-term aged bitumens while analyzing LAS test results. Their study proposed a fatigue resistance energy index (FREI) based on τ, which was conducted to determine the failure point of asphalt binders. However, τ is not suitable for identifying N_f. Cao and Wang [14] identified inconsistencies in the C × N and τ × N peaks as failure definition concepts to properly determine the N_f related to unaged, short-term aged, and long-term aged bitumens (NA and SBSB). Accordingly, their study proposed the $C^2 \times N \times (1 - C)$ peak as a new failure definition, thus resolving the issues. Zhang et al. [22] discovered inadequacies in ranking NA, SBSB, and polyphosphoric acid (PPA)-modified bitumen fatigue performances, which was achieved by considering aging conditions and N_f. Their study proposed a new parameter (but as it is based on τ, it is not convenient): the average reduction in C up to the failure point is used to determine N_f.

Lv et al. [23] confirmed that the stored PSE peak (failure definition) is suitable for identifying the N_f linked with long-term aged NA and self-healing polymer-modified bitumen (SPB). However, their study identified that bitumens with higher N_f failed to show greater fatigue behavior in terms of DCC analysis, demonstrating performance ranking inadequacies between the failure definition and DCC assessment. Furthermore, the use of $C^2 \times N \times (1 - C)$ and C × N failure concepts failed to properly determine the N_f associated with all the types of asphalt binder. These findings conflict with [14] and Safaei et al. [17].

Recently, Ilyin and Yadykova [24] proposed an extension of the Glover–Rowe parameter application, which includes the time–temperature superposition principle (TTSP) in the calculation process. These extension allows researchers to assess bitumen cracking behavior at low temperatures without conducting the test at the target temperature. However, ref. [25] confirmed that TTSP was not always applicable for evaluating the bitumen fatigue cracking performance.

The failure criterion (G^R) establishes a relationship between the material response and loading input [14], and it is the average rate of the released PSE when conducting the fatigue test up to the failure point. Wang et al. [8] presented the first study to apply the G^R concept to evaluate bitumen fatigue performance. Their research found a unique correlation between G^R and N_f, and it was found to be independent of loading history and temperature. Furthermore, their study applied the G^R concept, which was linked to the total released PSE ($W^R_{r,sum}$) as the sum of all released PSE (W^R_r) up to the failure point.

Safaei and Castorena [26] proved that the LAS temperature, to test polymer-modified bitumens (PMBs) and NA, should be carefully selected to avoid flow effects or adhesion loss, as well as to allow for convenient bitumen dynamic shear modulus values. Hence, temperature was included in the LAS test and S-VECD theory for assessing asphalt binder fatigue performance. Their study also found that the $G^R - N_f$ correlation was independent of the temperature and loading history. Wang et al. [9] proposed the introduction of the TTSP to eliminate the discovered effect of temperature on DCC analysis and G^R values when testing SBSB, terpolymer (TP)-modified bitumen, and NA. These findings conflicted with the findings of previous studies [8,26]. Moreover, the scholars detected an inconsistency between the failure definition and DCC analysis in terms of the bitumen fatigue performance ranking.

Cao and Wang [14] demonstrated that the G^R and N_f relationship and the $W^R_{r,sum}$ and N_f correlation were occasionally strong and poor, respectively, which can affect the actual understanding of G^R. As a result, their study proposed a new failure criterion based on a power law function between the sum of the stored PSE (W^R_{sum}) and a variable defined as the straining effort (SE). SE represents the effort required to damage the asphalt binder up to the failure point. The relationship between W^R_{sum} and SE was strong. Wang et al. [27] introduced a new type of failure criterion, where G^R was determined according to the total released pseudo-strain energy (TRPSE) as the area under the released PSE curve up to the failure point, which is used to improve the accuracy of bitumen fatigue analysis and prediction. Their study also introduced a new parameter: averaged released pseudo-strain energy per cycle ($\overline{W^R_r}$). This new G^R concept exhibits a strong correlation between G^R and N_f.

Chen et al. [25] discovered that, in some cases, the shift factor of TTSP was unable to eliminate the temperature effect on DCC. Accordingly, they proposed a simple procedure to determine the coefficients (C_1 and C_2) linked with the C-S power law function and estimate N_f at different temperatures, thereby representing an alternative to G^R. However, the new proposal was based on τ.

Lv et al. [23] assessed the efficacy of the power law function between W^R_{sum} and SE [14] and G^R in both terms of $W^R_{r,sum}$ [8], with TRPSE [27] as the failure criteria. Their study concluded that only a G^R based on TRPSE was able to properly accommodate the bitumen fatigue behavior, which confirms the superiority of this concept over the other two. Table 1 shows the 70# NA physical properties used in this study, which is the continuation of the research work of ref. [23].

Table 1. Physical properties of NA.

Test	Standard Value	Measured Value	Standard Test
Penetration (25 °C, 5 s, 100 g) (0.1 mm)	60~80	64.0	T0604
Penetration index (PI)	−1.5~1.0	−1.2	T0604
Softening point (°C)	≥46	48.5	T0606
Viscosity (60 °C) (Pa·s)	≥180	237	T0620
Ductility (10 °C) (cm)	≥15	25	T0605
Ductility (15 °C) (cm)	≥100	>150	T0605
Wax content (%)	≤2.2	1.8	T0615
Flash point (°C)	≥260	>300	T0611
Solubility (%)	≥99.5	99.91	T0607
Density (15 °C) (g/cm^3)	-	1.040	T0603
After the RTFO [1]:			
Mass change	≤±0.8	−0.034	T0609
Residual penetration ratio (%)	≥61	63.6	T0604
Residual ductility (10 °C) (cm)	≥6	6.3	T0605

[1] Rolling thin film oven (RTFO) test.

In summary, only the stored PSE peak as the failure definition and the G^R based on TRPSE were effective in accommodating bitumen fatigue behavior. However, the current failure definition and DCC analysis fail in consistently ranking a group of bitumen fatigue performances [9,23]. This inadequacy could define a key point in selecting the most convenient asphalt binder for a specific project.

Utilizing the S-VECD model for bitumen fatigue characterization comprises three main elements—linear viscoelastic (LVE) responses, DCC properties, and G^R determination—and all of them should be included in the final conclusion [9]. As a result, the S-VECD model elements should be consistent when analyzing bitumen fatigue performance, but with the current framework, it is hard to observe this requirement. Hence, developing a framework is necessary not only to match the abovementioned requirement, but also to accommodate the fatigue cracking behavior of any type of asphalt binder (NA or PMBs). Currently, the new procedure is being used to evaluate SPBs, which has been attracting the attention of researchers [28,29]. Our research team proposes that changing the foundational elements contained in the S-VECD model would make eliminating the ranking inconsistency possible. According to the previous comments, the objectives of this study are as follows:

- To develop a framework that addresses the ranking inconsistency between the failure definition and DCC analysis;
- To verify the developed framework's usefulness in evaluating bitumen fatigue cracking performance;
- To test NA and PMBs, including SPB, to verify our proposal's capability to accommodate the performance of any asphalt binder type.

2. Materials and Methods

2.1. Materials

2.1.1. Neat Asphalt Binder (NA)

This research used 70# NA from China Petroleum & Chemical Corporation (SINOPEC), Jinling Branch (Nanjing City, Jiangsu Province, China). This NA grade has shown high efficiency in withstanding the traffic loading cycle [30]; hence, it was expected that this study could successfully be carried out utilizing this bitumen. Table 1 shows NA's physical properties, which observe the required values. The standard tests in Table 1 are Chinese specifications based on AASHTO and ASTM specifications.

2.1.2. SBSB

SBS can improve the rutting performance, cohesion, adhesion, and elasticity properties of NA [31–33]. As a result, SBSB has become the global mainstream in modified bitumen, including in China [34]. Consequently, our research team decided to incorporate SBSB in this research. Table 2 shows the physical properties of SBSB.

Table 2. Physical properties of SBSB.

Test	Standard Value	Measured Value	Standard Test
Penetration (25 °C, 5 s, 100 g) (0.1 mm)	30~60	52.0	T0604
PI	$\geq$0	0.15	T0604
Softening point (°C)	$\geq$76	83.2	T0606
Viscosity (135 °C) (Pa·s)	$\leq$3	2.45	T0625
Ductility (5 °C) (cm)	$\geq$25	35	T0605
Flash point (°C)	$\geq$230	310	T0611
Solubility (%)	$\geq$99.0	99.78	T0607
SBS block ratio (B/S)	-	70/30	-
SBS molecular weight (g/mol)	-	120,000	-
SBS content (%)	-	5	-
After the RTFO:			
Mass change	$\leq\pm$1.0	$-$0.04	T0610
Residual penetration ratio (%)	$\geq$65	78	T0604
Residual ductility (10 °C) (cm)	$\geq$20	22	T0605

2.1.3. Self-Healing Elastomers

STP

This study is the continuation of previous research (Lv et al. [23]), where it was determined that the stored PSE peak as a failure definition and DCC analysis failed to show consistency in ranking bitumen fatigue performance. The research of Lv et al. [23] used a self-healing elastomer, which was classified as a room temperature (25 °C) self-reinforcing self-healing thermoplastic polyurethane (STP). Hence, STP was included in this study (received from Nanjing University).

The materials used in the synthesis of STP include polytetramethylene ether glycol (PTMEG, Mn = 1000 g/mol, f = 2), the catalyst dibutyltin dilaurate (DBTDL), and chain extender 3-Dimethylaminopropylamine (DMAPA), which were acquired from Aladdin. Isophorone di-isocyanate (IPDI) was purchased from Adamas. These reagents were utilized without further purification. Tetrahydrofuran (THF, Sigma-Aldrich, St. Louis, MO, USA) and chloroform ($CHCl_3$, Sigma-Aldrich) were utilized after CaH_2 redistillation.

STP comprises a crystallizable soft segment (PTMEG) of a well-selected length, which provides suitable efficiency for STP. This proper length of the soft segment guarantees a lower crystallization energy threshold when stretching the STP in the elongation test. Stratified H-bonding interactions are identified as bonds with sacrificial and dynamic characteristics, which ensure hard domains with low binding energy properties. Previous facts create conditions for a crystalline configuration with an active exchange in H-bonds when the STP is damaged. As a result, hard domain segments are likely to connect with small-sized hard domains through H-bonding, thereby promoting self-healing behavior without extra stimuli (microwave and heat), which is a convenient property for road surfaces. Moreover, STP has a strain-induced crystallization that guarantees a retarded but reversible self-reinforcing effect [35]. Figure 3 displays the synthesis process of STP and its chemical structure.

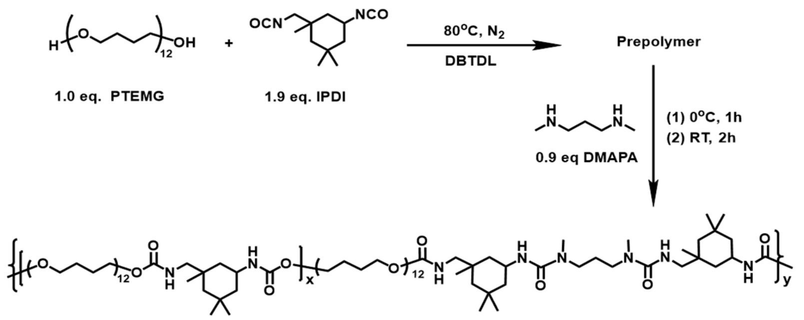

Figure 3. Synthesis process of STP and its chemical structure [23].

Table 3 shows the physical properties of STP. For more information about STP, such as—for example—its synthesis procedure and the materials used in this process, see Li et al. [35] and Lv et al. [23].

Table 3. Physical properties of STP.

Parameters	STP Values
Tensile strength (MPa)	13.5 ± 2.2
Elongation (dried state, %)	1460 ± 87
Density (g/cm^3)	1.07
Melting point (°C)	120 [a]
Molecular weight (g/mol)	72,700

[a] = obtained from the temperature sweeping of the rheological test.

IPA1w

Our research team included a second self-healing elastomer in this study for a comprehensive evaluation of the current framework's capacity to properly accommodate the fatigue performance of any type of PMB, even though it is a case of SPMB. The IPA1w was received from Nanjing University, and it is a polymer currently in the design stage. Additionally, IPA1w is a room temperature (25 °C) self-healing polymer that stimulates self-healing activity without extra stimuli (microwave and heat). This behavior could be suitable for road surfaces.

The material components used in the synthesis of IPA1w: Bis(3-aminopropyl)-terminated PDMS (M_n = 10,000 g mol^{-1}, noted as A1w) were purchased from Gelest. Isophorone diisocyanate (IPDI) was obtained from Sigma-Aldrich. Tetrahydrofuran (THF) was distilled for further use.

The synthesis of IPA1w: A1w (4.00 g, 0.4 mmol) was dissolved in redistilled THF (100 mL) and was continuously stirred in an ice bath for 30 min. Then, the solution of IPDI (91.13 mg, 0.41 mmol) in 30 mL of THF was slowly added into the mixture using a constant pressure funnel. The reaction mixture was stirred under a N_2 atmosphere for 24 h at room temperature and then concentrated into a sticky mucus. The product was purified using repeated dissolution–precipitation–decantation procedures. Finally, the concentrated solution was decanted into customized polytetrafluoroethylene molds and dried at 85 °C for 24 h. The resulting transparent IPA1w polymer film was then peeled off for further testing.

Bonding interactions and physical entanglements of the hydrogen were present in the polymer, and these properties produced its crosslinking sites. Hence, the self-healing phenomenon can be promoted by smashing and reconnecting the hydrogen bonds and/or disassembling and reassembling the polymer chains at room temperature. The polymer units with hydrogen bonds are more likely to connect their chains and provide entanglements [36]. Figure 4 illustrates the IPA1w self-healing process and its polymer structure "Reprinted/adapted with permission from Ref. [36] Copyright 2021, American Chemical Society".

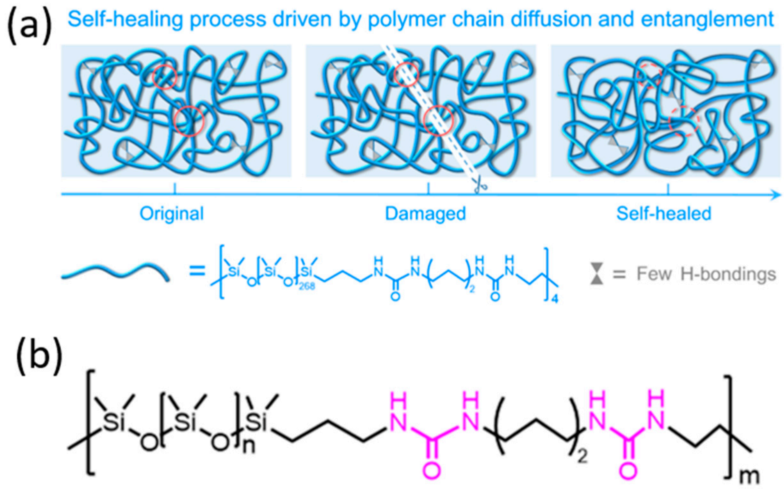

Figure 4. IPA1w information: (**a**) self-healing process and (**b**) molecular structure [36].

Table 4 shows the physical properties of IPA1w. For more detailed information about IPA1w, see Wang et al. [36].

Table 4. Physical properties of IPA1w.

Parameters	STP Values
Tensile strength (MPa)	1.61 ± 0.15
Elongation (dried state, %)	1700
Young's modulus (MPa)	0.59 ± 0.02
Toughness (MJ m^{-3})	17.89 ± 0.18
Molecular weight (g/mol)	82,000

2.2. Methods

2.2.1. Preparation of STP Modified Bitumen (STPB)

This study represents a continuation of the research in Lv et al. [23]; as a result, the mixing conditions and procedure from their research were followed to obtain STPBs.

Moreover, the 0.5, 1.0, and 1.5 wt% of STP were the amounts of polymer added to the NA to obtain STPB0.5, STPB1.0, and STPB1.5, respectively. The previous study utilized the 1, 3, and 5 wt% of STP as the amount of polymer added to the NA. Their results showed that the modified bitumen containing 1% of STP exhibited the best fatigue performance in terms of DCC analysis and self-restoration capacity. Additionally, this modified asphalt binder showed superior fatigue failure points in the C vs. S graph, regardless of the failure definition concepts. As a result, this new research work selected 0.5%, 1%, and 1.5% STP contents according to the previous experience in [23]. Figure 5 shows the general flowchart of all the procedures conducted in this study.

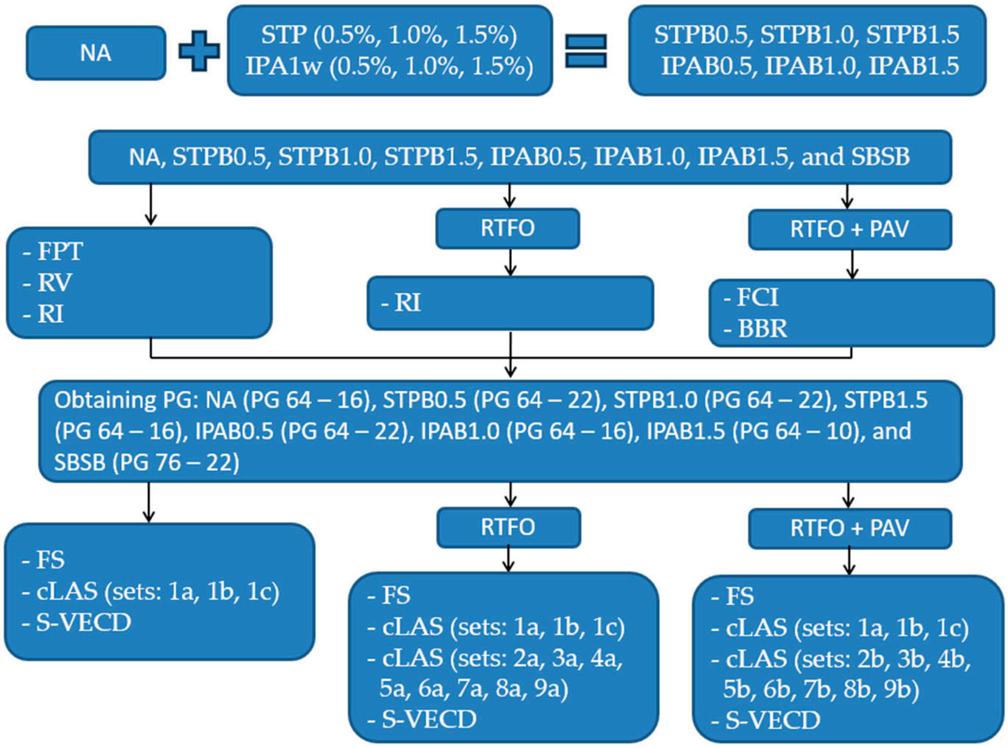

Figure 5. General flowchart of all the procedures performed in this study.

2.2.2. Preparation of IPA1w-Modified Bitumen (IPAB)

After numerous trial and error tests in the laboratory, our research team decided that the mixing conditions and procedure used for mixing STP and NA must be the same as those used for mixing IPA1w and NA. This decision was taken after analyzing the storage stability of IPABs according to ASTM-D7173 [37], and the procedure described in a previous study was also followed [38]. Hence, the results demonstrated that the IPABs showed good storage stability after mixing IPA1w and NA following the same procedure as was used for mixing STP and NA. This process was conducted because their research team did not have previous experience mixing IPA1w and NA. Additionally, 0.5%, 1.0%, and 1.5% were the amounts of polymer added to the NA to obtain IPAB0.5, IPAB1.0, and IPAB1.5, respectively. These percentages of IPA1w were selected according to the experience with similar percentages of self-healing materials in the study [39], where the modified bitumen showed higher self-restoration capacity, rutting resistance, and viscoelasticity. Furthermore, the previous experience of this research team [23] was also utilized for selecting the abovementioned percentages of IPA1w.

2.2.3. Aging Procedure

The rolling thin film oven (RTFO) test described in the AASHTO T240 [40] and the pressurized aging vessel (PAV) test explained in the AASHTO R28-12 [41] were utilized to conduct short-term and long-term aging procedures, respectively. NA, SBSB, STPB0.5, STPB1.0, STPB1.5, IPAB0.5, IPAB1.0, and IPAB1.5 were subjected to short-term and long-term aging procedures. Then, the unaged, RTFO-aged, and PAV-aged bitumen specimens in this study were tested according to the LAS test.

2.2.4. Performance Grade (PG) Characterization

A flash point temperature test (FPT) (AASHTO T48-06) [42] and rotational viscosity test (RV) (AASHTO T316) [43] were conducted on unaged asphalt binders. The rutting index (RI) (AASHTO T315-20) [44] was obtained for RTFO-aged and -unaged bitumens. The fatigue cracking index (FCI) (AASHTO T315-20) [44] and bending beam rheometer test (BBR) (AASHTO T313-12) [45] were carried out on RTFO + PAV-aged bitumens. These experiments were undertaken to determine the PG of NA, SBSB, STPB0.5, STPB1.0, STPB1.5, IPAB0.5, IPAB1.0, and IPAB1.5. AASHTO M320-10 [46] was used to define the PG of all the bitumens. The obtained PGs were as follows: NA (PG 64-16), SBSB (PG 76-22), STPB0.5 (PG 64-22), STPB1.0 (PG 64-22), STPB1.5 (PG 64-16), IPAB0.5 (PG 64-22), IPAB1.0 (PG 64-16), and IPAB1.5 (PG 64-10).

2.2.5. LAS Test

The LAS test comprises a frequency sweep test (FS) and continuous LAS test (cLAS). The former test was conducted at a frequency range of 0.1–100 rad/s and a strain level equal to 0.1%—which were performed at different temperatures (T) (i.e., 20 °C, 25 °C, 30 °C, 35 °C, and 40 °C)—in order to determine the master curve and the damage evolution rate "α". The latter test was carried out at a frequency of 10 Hz, and the linear strain amplitude was ramped up from 0.1% to 30% for 3100 cycles. Both test types (FS and cLAS) were conducted by utilizing an 8 mm plate (plate/plate) with a 2 mm gap. For more details about these tests, see Lv et al. [23]. All the bitumens in this study at different aging stages (unaged (U), RTFO-aged (R), and RTFO + PAV-aged (RP)) were subjected to the abovementioned tests. In this study, the cyclic strain rate (CSR) ranged from 0.006 to 0.030. The CSR represents the quotient between the highest strain (always 30%) and the number of cycles, such as—for instance—the standard CSR being the 30%/3100 $\approx$ 0.010%/cycle. The temperature for carrying out the cLAS test was set as follows: determine the average of the low and high PG temperatures of each asphalt binder and then add 4 °C [47]. As a result, the temperature was set to be 25 °C, 28 °C, and 31 °C. Tables 5 and 6 show the fatigue test matrix, including the CSRs and test temperatures associated with the "validation of failure definition" (VFD) and "validation of failure criterion" (VFC), respectively. These conditions were decided according to previous studies [8,14] and the previous experience of Lv et al. [23].

Table 5. Fatigue test matrix for the failure definition validation.

Set	Material Name (MN)	PG	Aging Condition (AC)	CSR (%/Cycle)	T (°C)	Note
1a	NA, STPB1.5, IPAB1.0	64-16	U, R, RP	0.010	25	VFD
	STPB0.5, STPB1.0, IPAB0.5	64-22	U, R, RP	0.010	25	VFD
	IPAB1.5	64-10	U, R, RP	0.010	25	VFD
	SBSB	76-22	U, R, RP	0.010	25	VFD
1b	NA, STPB1.5, IPAB1.0	64-16	U, R, RP	0.010	28	VFD
	STPB0.5, STPB1.0, IPAB0.5	64-22	U, R, RP	0.010	28	VFD
	IPAB1.5	64-10	U, R, RP	0.010	28	VFD
	SBSB	76-22	U, R, RP	0.010	28	VFD
1c	NA, STPB1.5, IPAB1.0	64-16	U, R, RP	0.010	31	VFD
	STPB0.5, STPB1.0, IPAB0.5	64-22	U, R, RP	0.010	31	VFD
	IPAB1.5	64-10	U, R, RP	0.010	31	VFD
	SBSB	76-22	U, R, RP	0.010	31	VFD

Table 6. Fatigue test matrix for the fatigue criterion validation.

Set	MN	PG	AC	CSR (%/Cycle)	T (°C)	Note
2a	NA	64-16	R	0.010 [1], 0.030 [2], 0.015 [3], 0.006 [4]	28 [1], 32 [2], 26 [3], 30 [4]	VFC
2b	NA	64-16	RP	0.010 [1], 0.0085 [2], 0.0075 [3], 0.020 [4], 0.012 [5]	28 [1,2,3], 24 [4], 31 [5]	VFC
3a	STPB0.5	64-22	R	0.010 [1], 0.030 [2], 0.0085 [3], 0.015 [4]	25 [1], 26 [2], 24 [3], 27 [4]	VFC
3b	STPB0.5	64-22	RP	0.010 [1], 0.030 [2], 0.0075 [3], 0.015 [4], 0.0085 [5]	25 [1], 22 [2,3], 27 [4], 28 [5]	VFC
4a	STPB1.0	64-22	R	0.010 [1], 0.015 [2], 0.006 [3], 0.030 [4]	25 [1], 27 [2], 29 [3], 24 [4]	VFC
4b	STPB1.0	64-22	RP	0.010 [1], 0.0085 [2], 0.0075 [3], 0.0066 [4], 0.012 [5]	25 [1,2], 27 [3,4], 23 [5]	VFC
5a	STPB1.5	64-16	R	0.010 [1], 0.020 [2], 0.012 [3], 0.0085 [4]	28 [1,2], 26 [3], 31 [4]	VFC
5b	STPB1.5	64-16	RP	0.010 [1], 0.0066 [2], 0.0085 [3], 0.030 [4], 0.015 [5]	28 [1], 25 [2,3], 28 [4], 30 [5]	VFC
6a	IPAB0.5	64-22	R	0.010 [1], 0.020 [2], 0.0066 [3], 0.030 [4]	25 [1,2], 23 [3], 27 [4]	VFC
6b	IPAB0.5	64-22	RP	0.010 [1], 0.020 [2], 0.0085 [3], 0.012 [4], 0.006 [5]	25 [1,2], 27 [3], 28 [4], 23 [5]	VFC
7a	IPAB1.0	64-16	R	0.010 [1], 0.012 [2], 0.0066 [3], 0.015 [4]	28 [1,3], 30 [2], 26 [4]	VFC
7b	IPAB1.0	64-16	RP	0.010 [1], 0.012 [2], 0.0085 [3], 0.030 [4], 0.0066 [5]	28 [1], 30 [2], 31 [3], 26 [4], 25 [5]	VFC
8a	IPAB1.5	64-10	R	0.010 [1], 0.030 [2], 0.020 [3], 0.0085 [4]	31 [1,3], 29 [2], 34 [4]	VFC
8b	IPAB1.5	64-10	RP	0.010 [1], 0.030 [2], 0.012 [3], 0.0085 [4], 0.0075 [5]	31 [1], 33 [2], 29 [3], 28 [4], 34 [5]	VFC
9a	SBSB	76-22	R	0.010 [1], 0.012 [2], 0.0066 [3], 0.030 [4]	31 [1], 30 [2], 28 [3], 33 [4]	VFC
9b	SBSB	76-22	RP	0.010 [1], 0.0066 [2], 0.0085 [3], 0.015 [4], 0.020 [5]	31 [1], 34 [2], 29 [3], 32 [4], 27 [5]	VFC

Note: CSR and T values with the same superscript are included in the same test conditions inside the corresponding set. The T values with two or more superscripts mean that T is the same for the corresponding CSR with the same superscript.

2.2.6. S-VECD

The S-VECD model was used to process the LAS test results. This model effectively determines the C and S values, and its relationship is independently correlated to the loading history, regardless of the asphalt binder. As a result, it is possible to determine numerous bitumen fatigue responses under any decided conditions with few experimental data [8,26,48]. The DCC can be built by utilizing the S-VECD, and this special curve represents the correlation between C and S (see Equation (2)) [8]. In this study, C and ΔS (damage increment) were determined using Equations (3) and (4), respectively [14]:

$$C = 1 - C_1\left(S^{C_2}\right) \; with \; S = \sum_{i=1}^{S_f} \Delta S_i, \tag{2}$$

$$C = \frac{|G^*|}{|G^*|_{LVE} \cdot DMR} \; with \; DMR = \frac{|G^*|_{fingerprint}}{|G^*|_{LVE}}, \tag{3}$$

$$\Delta S_i = \left(\frac{1}{2} DMR \cdot \left(\gamma_i^R\right)^2 \cdot (C_{i-1} - C_i)\right)^{\frac{\alpha}{1+\alpha}} \cdot Q \quad with \; Q \equiv \left[\int (sin(\omega_r \vartheta))^{2\alpha} d\vartheta\right]^{\frac{1}{1+\alpha}}, \tag{4}$$

where C_1 and C_2 are the regression constants, and S_f is the S value at the failure point (Equation (2)). In the case of Equation (3), G^*, $|G^*|_{LVE}$, DMR, and $|G^*|_{fingerprint}$ represent the dynamic shear modulus (damaged), undamaged dynamic shear modulus (linear viscoelastic range (LVE)), dynamic modulus ratio, and the initial dynamic shear modulus when conducting cLAS, respectively. Moreover, γ_i^R, ω_r, ϑ, and i-th in Equation (4) correspond to the pseudo-strain amplitude, reduced angular frequency, reduced time, and the cycle of interest, respectively. Equations (5) and (6) illustrate how to determine the W^R (stored PSE) and γ_i^R, respectively [14].

$$W^R = \frac{1}{2} DMR \cdot C(S) \cdot \left(\gamma^R\right)^2, \tag{5}$$

$$\gamma_i^R(\vartheta) = \gamma_i \cdot |G^*|_{LVE} \cdot sin(\omega_r \vartheta), \tag{6}$$

where γ_i represents the shear strain amplitude in Equation (6).

The stored PSE peak was the failure definition used in this study to evaluate the bitumen fatigue performance according to the proposal of Wang et al. [8] and the previous experience of Lv et al. [23] (see Figure 6).

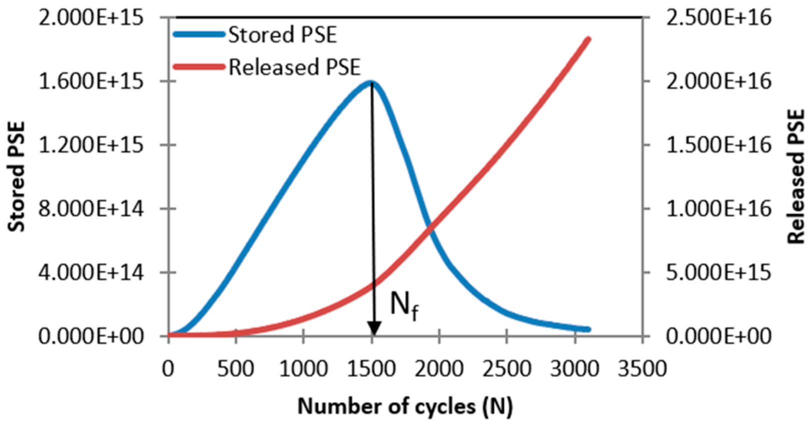

Figure 6. PSE-based failure definition (N_f = number of loading cycles up to the failure point) as per Lv et al. [23].

Moreover, the failure criterion used to introduce the average rate of the released PSE, which is based on the total released PSE (TRPSE) in terms of the area under the released PSE curve up to the failure point (see Figure 5), was used in this study according to the proposal from Wang et al. [27] and the previous experience of Lv et al. [23]. The equations are as follows:

$$G^R = \beta\left(N_f\right)^{\partial}, \tag{7}$$

$$W_r^R = \frac{1}{2} DMR \cdot (1 - C_i)\left(\gamma_i^R\right)^2, \tag{8}$$

$$G^R = \frac{\overline{W_r^R}}{N_f} = \frac{TRPSE/N_f}{N_f} = \frac{TRPSE}{\left(N_f\right)^2}, \tag{9}$$

where β and ∂ are the regression constants (in Equation (7)). For more detailed information about the failure definition and failure criterion in this study, see Lv et al. [23].

2.2.7. Developing a Framework to Determine the Failure Definition and Failure Criterion

As mentioned before, the current failure definition (the stored PSE peak) used to identify N_f and DCC analysis was not consistent in ranking a group of bitumens in terms of the fatigue behavior [9,23]. Bitumen fatigue characterization utilizing the S-VECD model comprises three elements based on the linear viscoelastic (LVE) responses, DCC properties, and the failure criterion determination. As a result, the final conclusion on the bitumen fatigue performance must include all these elements and not simply two of them [9]. Accordingly, this research team proposes the following framework.

Theoretical framework:

Total potential cohesion (TPC): A parameter that measures the imaginary bitumen strength capacity at each loading cycle to maintain its C values equal to 1 when conducting the cLAS test, even when damage has occurred. It is an imaginary rectangular area that is defined by A, B, F, and E in Figure 7, and it can be obtained from any bitumen to represent its imaginary fatigue stage at any loading cycle. The AB side of the imaginary rectangular area represents a segment of the imaginary damage characteristic curve (I-DCC), which is obtained when the asphalt binder is subjected to the cLAS test, as well as by keeping the C values equal to 1, even if damage has occurred. The TPC can be determined in each loading cycle, and the equation is as follows:

$$TPC_i = S_i \cdot C_0 \ (where \ C_0 = 1), \tag{10}$$

where TPC_i, S_i, and C_0 are the total potential cohesion at the i-th cycle, the S value at the i-th cycle, and the constant material integrity equal to 1, respectively.

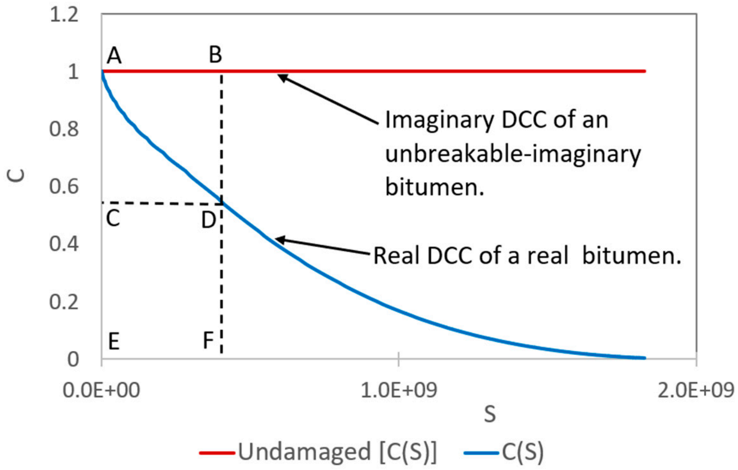

Figure 7. Representation of the imaginary and real DCC.

Stored potential cohesion (SPC): A parameter that measures the bitumen strength capacity at each loading cycle to maintain as high C values as possible when conducting the cLAS test, even when damage has occurred. It is the rectangular area defined by C, D, F, and E in Figure 7, and it can be obtained from any bitumen to represent its fatigue stage at any loading cycle. The SPC is determined by the product of the C value (ordinate axis) and the S value (abscissa axis), and it is linked with any loading cycle on the real DCC (DCC), which represents the real fatigue performance stage of the asphalt binder at the selected loading cycle. Its equation is as follows:

$$SPC_i = S_i \cdot C_i, \tag{11}$$

where SPC_i and C_i are the stored potential cohesion and the C value at the i-th cycle, respectively.

Released potential cohesion (RPC): A parameter that measures the dissipated bitumen strength capacity at each loading cycle to maintain C values as high as possible when conducting the cLAS test. It is the rectangular area that is defined by A, B, D, and C in Figure 7, and it can be obtained from any bitumen. The RPC equation is as follows:

$$RPC_i = TPC_i - SPC_i, \tag{12}$$

where RPC_i is the released potential cohesion at the i-th cycle.

Figure 8 illustrates the potential cohesion (PC) and the damage evolution in the cLAS test. The imaginary undamaged line represents the imaginary material response if its integrity is equal to 1, even when the damage increases, and the area below this line shows the sum of each TPC related to each loading cycle. The real material response deviates from the imaginary undamaged line. The area below the real material response represents the sum of each SPC linked with each loading cycle, and the area between the real material response and the imaginary undamaged line shows the sum of each RPC associated with each loading cycle. Figure 9 depicts the SPC and RPC graphs. When the SPC increases, the bitumen still has the strength capacity to store additional damage when conducting the cLAS test (loading amplitude/energy input increases). However, if the SPC decreases, the asphalt binder is no longer able to sustain additional damage in the cLAS test; hence, bitumen failure occurs. As a result, the peak of the SPC is proposed as a failure definition, and S_f defines the S value at which the failure occurs, as mentioned before. Furthermore, higher SPC values represent superior fatigue performance at the selected loading cycle. The RPC continuously increases from the beginning of the test (i.e., the material loses strength capacity from the starting point).

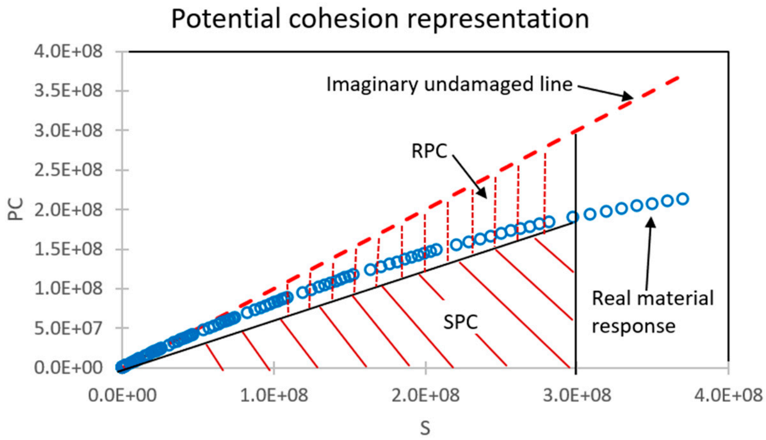

Figure 8. Potential cohesion representation.

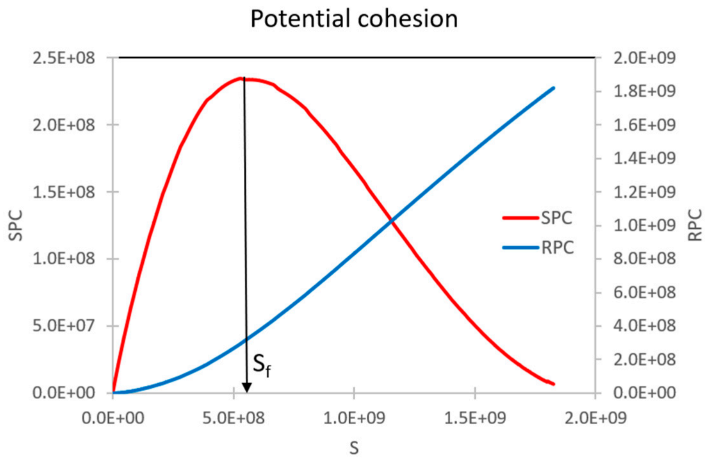

Figure 9. Stored and released potential cohesion graphs.

The average rate of the released potential cohesion during the cLAS test up to the macro-cracking localization within the material is defined as C^R, and its equation is as follows:

$$C^R = \frac{C_R^P}{\left(S_f\right)^2}, \quad (13)$$

where C_R^P is the sum of all RPC values up to the failure point defined by S_f; its equation is as follows:

$$C_R^P = \sum_{i=1}^{S_f} RPC_i, \quad (14)$$

Accordingly, this research team proposes the following relationship as the failure criterion:

$$C^R = k \times \left(S_f\right)^d. \quad (15)$$

This research team proposes the following concept: cohesion work (CW). This parameter shows a general assessment of bitumen fatigue performance up to the point where the CW is obtained. The CW can be calculated as the area below the DCC (CW_{DCC}) or as the area below the SPC curve (CW_{SPC}). The CW_{DCC} and CW_{SPC} can be determined before, after, and at the failure point of any bitumen. The equation related to both parameters are as follows:

$$CW_{DCC} = \int_0^{S_m} 1 - C_1\left(S^{C_2} + C_3\right), \tag{16}$$

$$CW_{SPC} = \int_0^{S_m} aS^3 + bS^2 + cS + d, \tag{17}$$

where C_1, C_2, C_3, a, b, c, and d are regression coefficients, and S_m is the S value at the point at which the calculation is conducted. Higher values of CW_{DCC} and CW_{SPC} mean superior fatigue performance in terms of DCC analysis and SPC curve assessment, which are needed to withstand higher levels of damage intensity.

Equation (16) was selected according to the previous experience in the research of Lv et al. [23] to obtain a superior fitting with respect to the DCC. Equation (17) was selected after numerous trial and error tests. Obtaining a fitting equation that can precisely accommodate the DCC and SPC curve is convenient for determining high-quality results. This research team used the "solver" option in Microsoft Excel (version 2312).

3. Results

3.1. Failure Definition Evaluation

Figures 10–12 illustrate the DCCs of all the bitumens related to test sets 1a, 1b, and 1c, respectively. These figures demonstrate that IPAB0.5, STPB0.5, and STPB1.0 generally exhibit greater fatigue performance than the other bitumens in this study because their C values were found to be higher than those related to other bitumens regardless of the S values. This means that IPAB0.5, STPB0.5, and STPB1.0 can withstand the same damage intensity with superior material integrity. In the case of long-term aging (Figures 10c, 11c and 12c), IPAB0.5 and STPB1.0 mainly showed superior fatigue performance compared to the other bitumens, which means these asphalt binders would provide longer service life, in terms of DCC analysis, if both were used in road construction.

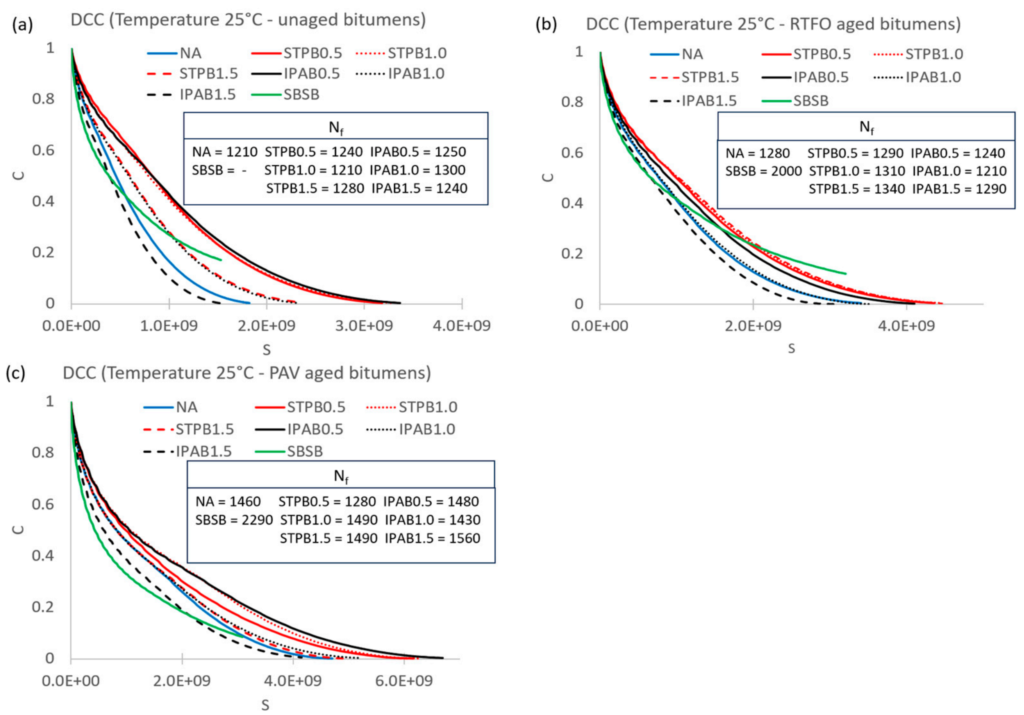

Figure 10. The DCCs of the bitumens related to 25 °C at different aging conditions: (**a**) unaged bitumens; (**b**) RTFO-aged bitumens; and (**c**) PAV-aged bitumens.

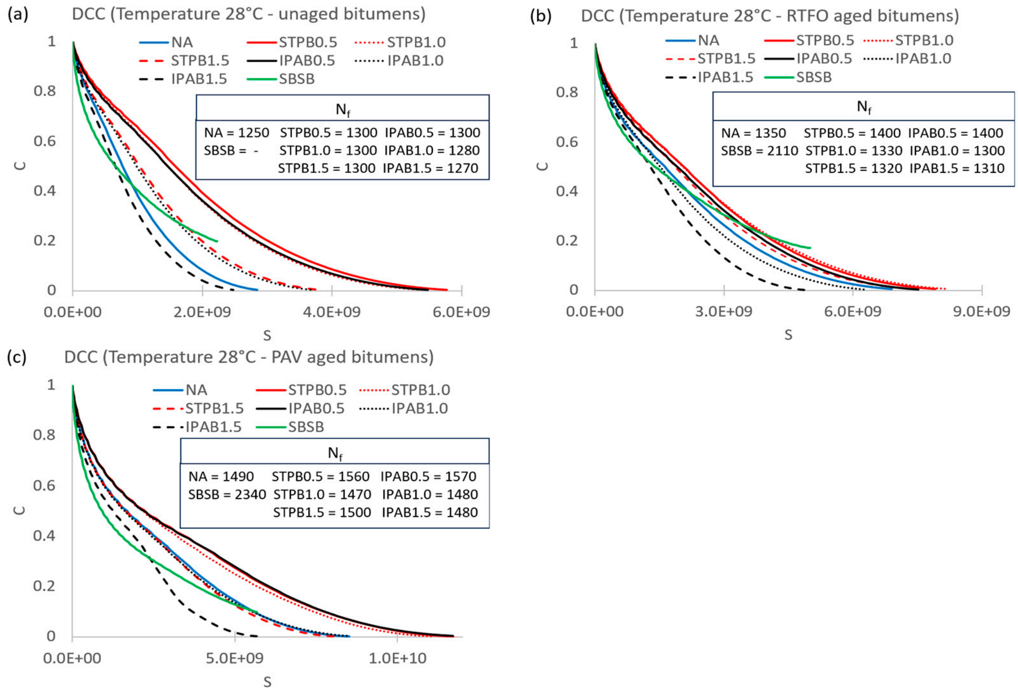

Figure 11. The DCCs of the bitumens related to 28 °C at different aging conditions: (**a**) unaged bitumens; (**b**) RTFO-aged bitumens; and (**c**) PAV-aged bitumens.

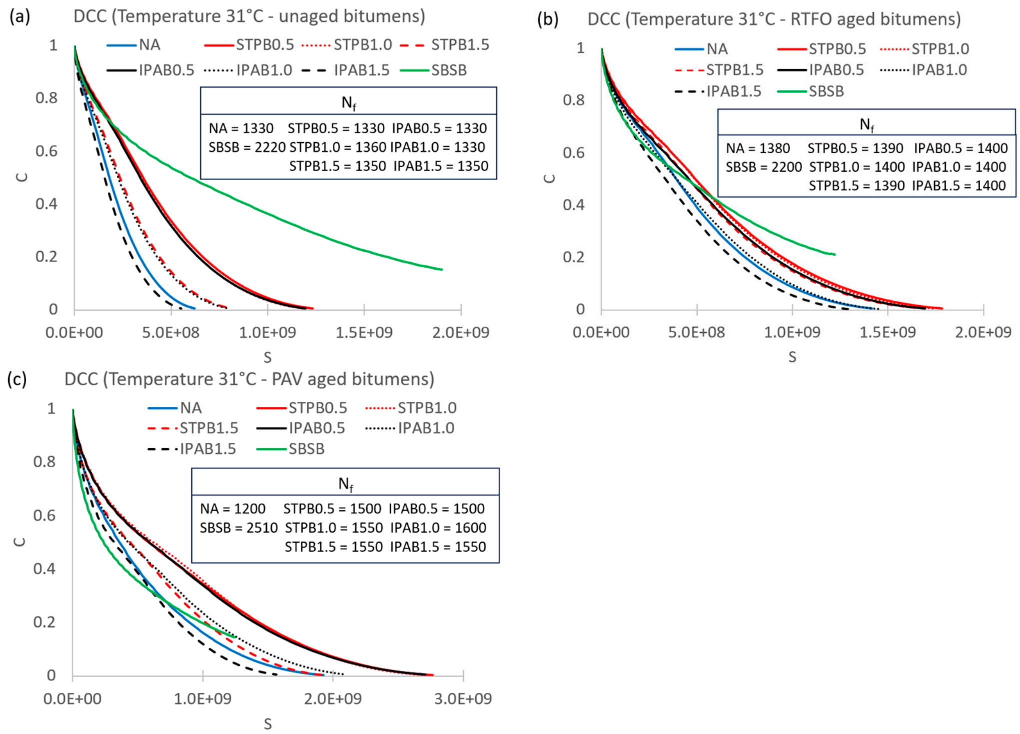

Figure 12. The DCCs of the bitumens related to 31 °C at different aging conditions: (**a**) unaged bitumens; (**b**) RTFO-aged bitumens; and (**c**) PAV-aged bitumens.

Figures 10–12 also display the N_f linked with all the bitumens at different aging stages at 25 °C, 28 °C, and 31 °C, respectively. These figures prove that SBSB, STPB1.5, and STPB1.0 commonly exhibit N_f values within the top three highest values associated with each section in each figure. This means that these bitumens must usually be subjected to a higher number of loading cycles to reach the failure point, regardless of the temperature and aging conditions. SBSB exhibits the highest N_f in long-term aging analysis: 2290, 2340, and 2510 at 25 °C, 28 °C, and 31 °C, respectively. The N_f values were obtained by utilizing the conventional failure definition (stored PSE peak). See "Supplementary Materials", Figure S1, which shows the stored PSE curves of the bitumens at different temperature and aging conditions. It can be seen that the bitumens with superior fatigue behavior according to DCC interpretation are different from the asphalt binders that exhibit greater fatigue performance in terms of the N_f values, except in one case (STPB1.0). This finding agrees with previous studies [9,23]. As a result, the findings from this study and previous research works highlight the ranking inconsistency between the stored PSE peak (failure definition N_f) and the fatigue performance conforming to DCC analysis. This fact confirms the need for developing a new framework to overcome this issue.

Moreover, it can be seen in Figures 10–12 that the SBSB regularly shows lower C values than the other bitumens, regardless of the S values, which means the SBSB exhibits lower fatigue performance than the other bitumens (according to the DCC interpretation). These figures illustrate the same phenomenon seen in previous research works, such as in—for instance—Safaei et al. [3], Wang et al. [8], and Wang et al. [9]. But, with respect to N_f, (see Figure 10, Figure 11, Figure 12 and Figure S1), SBSB always exhibited the highest values, except in the case of Figure S1a (or Figure 10a) and Figure S1d (or Figure 11a). This means that the SBSB must usually be subjected to the highest number of loading cycles to reach its failure point. Hence, the findings from this research work and previous investigations highlight the abovementioned inconsistency and demonstrate the need for a new procedure to eliminate the found inadequacy.

In Figure S1a,d, the N_f linked with SBSB cannot be identified because its stored PSE curve did not have a peak to identify this value. Hence, it is not possible to determine the fatigue performance of SBSB in terms of the number of loading cycles to reach the failure point. As a result, the stored PSE is not a useful parameter for assessing bitumen fatigue performance under any type of condition. To analyze the reason for this phenomenon (lack of peak in the stored PSE curve), it is necessary to analyze the stored PSE equation (see Equation (5)), and this formula mainly depends on the C and γ_i^R values. After a comprehensive analysis of both the parameter values, we concluded that the γ_i^R values increased at a high rate and that C keeps its values high enough to maintain the stored PSE curve's increase (without defining a peak) while undertaking the cLAS test. Accordingly, it is not possible to determine N_f under this condition.

Figures S2–S9 (see "Supplementary Materials") illustrate the DCCs of NA, STPB0.5, STPB1.0, STPB1.5, IPAB0.5, IPAB1.0, IPAB1.5, and SBSB at different respective temperature and aging conditions. It is interesting to note that all the bitumens showed their highest, middle, and lowest fatigue performance in terms of the DCC interpretation at 28 °C, 25 °C, and 31 °C, respectively, regardless of the aging condition (except as in Figure S9a, where the SBSB exhibited its highest, middle, and lowest fatigue performance at 31 °C, 28 °C, and 25 °C, respectively). This finding led to the inference that there must be a specific temperature (which is different for each bitumen) to reach the utmost bitumen fatigue performance in terms of DCC evaluation (i.e., higher C values regardless of S values). The DCC positions in the abovementioned C vs. S graphs were in conflict with the findings in a previous study by Wang et al. [9]. This previous research work proposed the application of TTSP by considering that the temperature causes the proportion location of DCC inside C vs. S graphs, but the findings from Figures S2–S9 disagree with that statement. These findings from the present study highlighted that TTSP, under certain conditions, does not apply to the DCC proportion location; therefore, the use of this principle should be meticulously considered so as to avoid a wrong analysis of bitumen fatigue performance. This conclusion agrees with a previous study by Chen et al. [25] (see detailed analysis of this finding in the section "4. Discussion").

Furthermore, Figures S2–S8 generally depict the PAV-aged, RTFO-aged, and unaged bitumens as numbers one, two, and three, respectively, in terms of fatigue performance according to DCC assessment and regardless of temperature. This finding does not correlate with actual engineering experience because PAV-aged asphalt binder should exhibit the worst fatigue behavior and RTFO-aged bitumen should show a lower performance than unaged bitumen. The conclusions from those figures agree with previous research, such as in—for instance—Chen and Bahia [49], Cao and Wang [14], and Zhou et al. [21]. The findings from this study and previous research works highlight the incapability of the current framework in properly depicting the DCCs in the C vs. S graph according to the aging conditions and practical experience in road engineering. In the case of Figure S9d,e, the unaged asphalt binder exhibited the worst behavior, and the RTFO-aged bitumens showed better performance than the PAV-aged bitumens. Only Figure S9f illustrates the fatigue performance in the order expected from the actual road engineering experience, which was unaged asphalt binder, RTFO-aged bitumen, and PAV-aged bitumen, which showed the number one, two, and three performances, respectively, in terms of the fatigue behavior according to the DCC placement in the C vs. S graph.

3.2. Failure Criterion Evaluation

Figures 13 and 14 illustrate the failure criterion related to the RTFO-aged and PAV-aged bitumens, respectively. Figure 13 is related to the test sets 2a, 3a, 4a, 5a, 6a, 7a, 8a, and 9a, and Figure 14 is linked with the test sets 2b, 3b, 4b, 5b, 6b, 7b, 8b, and 9b. Figures 13 and 14 generally exhibit the existence of a strong relationship between G^R and N_f regardless of the bitumens and experimental conditions, and this is because the R^2 values were often greater than 0.90. As a result, it was possible to confirm that the failure criterion based on the area below the stored PSE curve can usually predict the fatigue performance of asphalt binders under different test conditions—at least for those selected in this study. Nevertheless, the mentioned failure criterion was not useful in predicting the NA and IPAB0.5 fatigue performances under the selected test conditions linked with set 2a (Figure 13a) (former bitumen), as well as sets 6a (Figure 13c) and 6b (Figure 14c) (latter bitumen), because the R^2 values were low. The R^2 values related to sets 2a and 6a were extremely low. Hence, this finding highlighted that the current failure criterion according to the average rate of released PSE, which is based on TRPSE in terms of the area under the released PSE curve up to the failure point, is not a robust tool for predicting bitumen fatigue behavior under any type of test condition. As a result, the need to develop a new failure criterion arises. This conclusion conflicts with a previous study by Wang et al. [27].

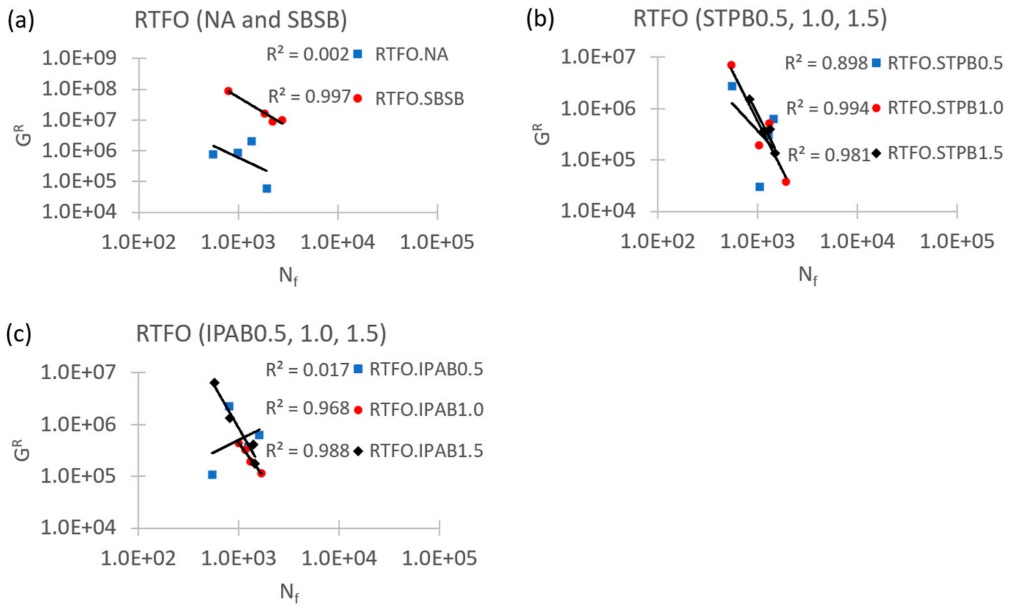

Figure 13. The G^R vs. N_f graph of RTFO-aged bitumens: (**a**) NA and SBSB; (**b**) STPB 0.5-1.0-1.5; and (**c**) IPAB 0.5-1.0-1.5.

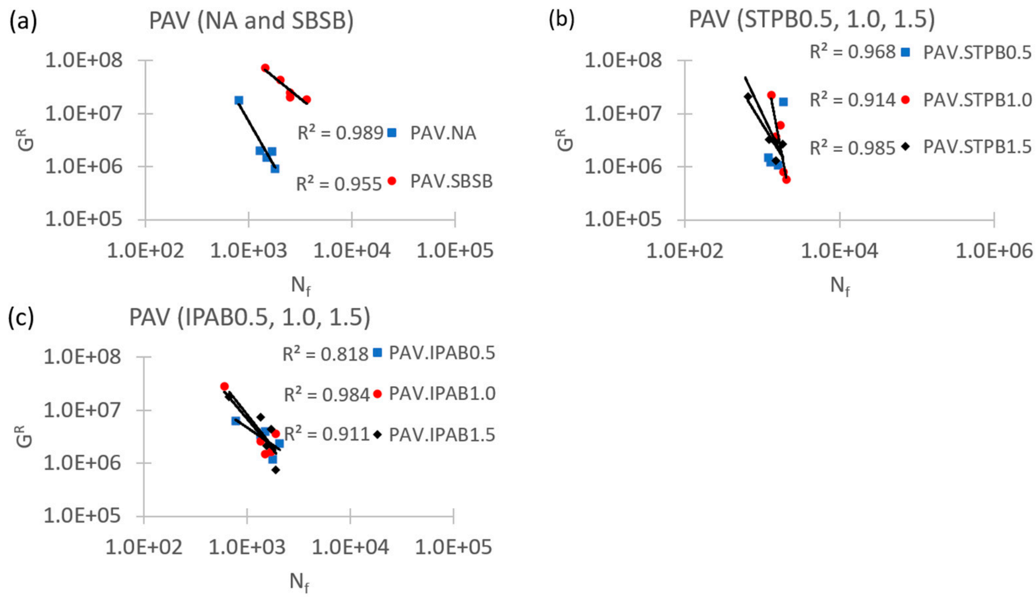

Figure 14. The G^R vs. N_f graph of PAV-aged bitumens: (**a**) NA and SBSB; (**b**) STPB 0.5-1.0-1.5; and (**c**) IPAB 0.5-1.0-1.5.

Furthermore, the slopes of the fitting graphs in Figures 13 and 14 are generally quite different. This means that the failure criterion based on the TRPSE in terms of the area under the released PSE curve up to the failure point identifies different tendencies in terms of how the average rate of released PSE changes while conducting the cLAS test. Moreover, this proves that the bitumen aging condition and the type of asphalt binder modifier have a high influence on how G^R values change—at least for the selected test conditions, bitumens, and asphalt modifiers—according to the abovementioned failure criterion.

3.3. Failure Definition Evaluation (New Proposal)

Figure S10 (see Supplementary materials) shows the failure definition points identified using the W^R peak (N_f) and SPC peak (S_f) on the W^R curves at different temperature and aging conditions. This figure proves that N_f and S_f are closely located on the W^R curves regardless of the bitumen, temperature, and aging conditions, which evidences that both concepts are compatible in terms of determining the failure point, even though these failure definitions have different basements. This demonstrates the efficacy of the new proposal of failure definition (SPC peak), at least for the bitumen, temperature, and aging conditions in this study. We realize that S_f is almost always at the right side of the N_f on the W^R curves regardless of the bitumen, temperature, and aging conditions, which means that the new proposal of failure definition identifies slightly longer service life for the bitumens in this study. The only case where the S_f is placed at the left side of the N_f on the W^R curve is in Figure S10i for SBSB.

Moreover, Figure S10 illustrates that N_f and S_f are closer when determining the failure point linked with PAV-aged bitumens than in the case of RTFO-aged and unaged asphalt binders, and this is regardless of the bitumens and temperatures. This proves that failure concepts agree better in terms of identifying the failure points of bitumens with a long time of service, at least for the selected test conditions and bitumens selected in this study. The new proposal of a failure definition solves the ineffectiveness of the traditional failure concept (W^R peak) in determining N_f under certain conditions (see Figure S1a,d associated with SBSB). As a result, Figure S10a,d depict the failure point on the W^R curve related to SBSB.

Figures 15–17 illustrate the DCCs with failure points (S_f) that were identified using the SPC peak at 25 °C, 28 °C, and 31 °C, respectively. Moreover, these figures are linked with test sets 1a, 1b, and 1c, respectively. Figures 15 and 16 show that bitumens with higher

S_f fail to exhibit greater fatigue performance in terms of DCC interpretation. For instance, Figure 15a,b and Figure 16b exhibit SBSB with a higher S_f than the other asphalt binders in this study. However, this bitumen fails to show a superior fatigue performance concerning STPB0.5, STPB1.0, and IPAB0.5 (in Figures 15a and 16b) and when compared with STPB0.5, STPB1.0, and STPB1.5 (in Figure 15b), in terms of the DCC evaluation. This is because the DCC linked with SBSB is always below the DCCs related to these bitumens in the mentioned figure sections.

Figure S11 depicts the SPC and RPC curves associated with all asphalt binders at different temperature and aging conditions. Figure S11a,b,e illustrate the SPC and RPC curves linked with DCCs in Figure 15a,b and Figure 16b, respectively. Figure S11a,e show that the SPC curves related to STPB0.5, STPB1.0, and IPAB0.5, even at the failure stage (after their corresponding peaks) were above the SPC curve linked with SBSB before and at its corresponding peak. This means that even STPB0.5, STPB1.0, and IPAB0.5 at the failure stage can show superior fatigue performance over SBSB without reaching the failure point (according to the SPC curve interpretation). Figure S11b illustrates that the SPC curves related to STPB0.5, STPB1.0, and STPB1.5, even though at the failure stage (at the right side of corresponding peaks), were above the SPC curve associated with SBSB before and at its corresponding peak. Hence, even though STPB0.5, STPB1.0, and STPB1.5 were in the failure stage, they exhibited better fatigue performance than SBSB without achieving its failure point in terms of the SPC curve evaluation.

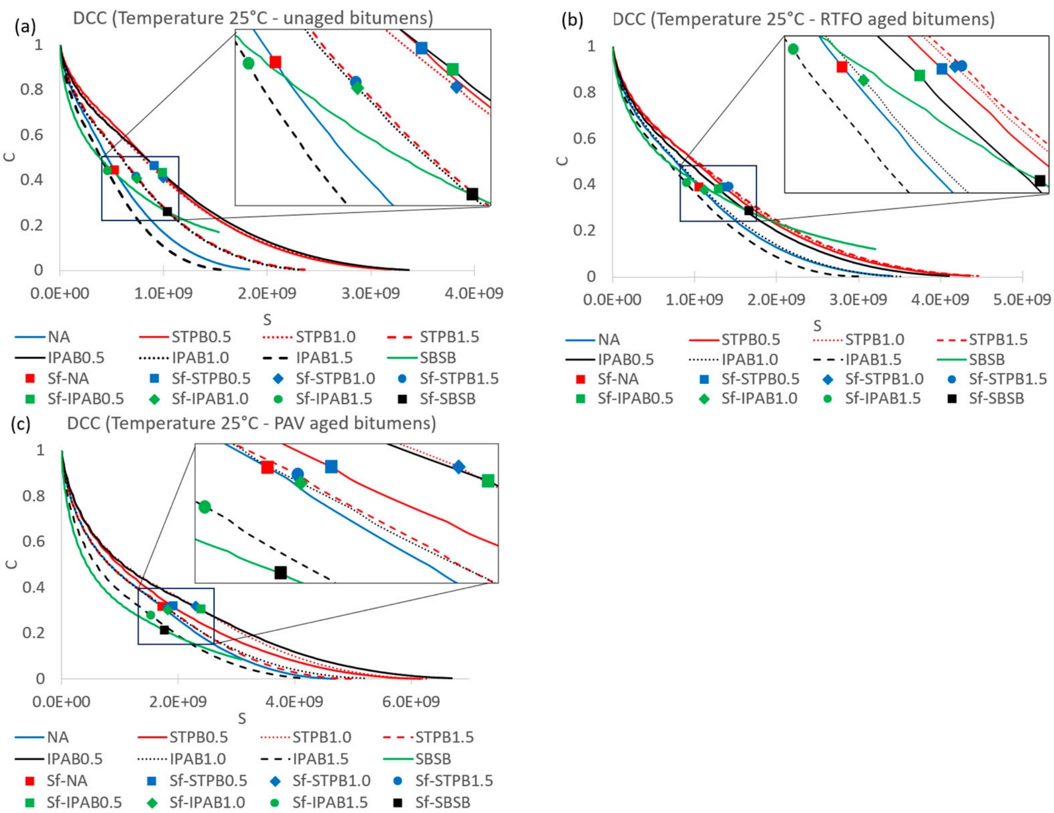

Figure 15. The DCCs with failure points identified using the peak of SPC at 25 °C: (**a**) unaged bitumens; (**b**) RTFO-aged bitumens; and (**c**) PAV-aged bitumens.

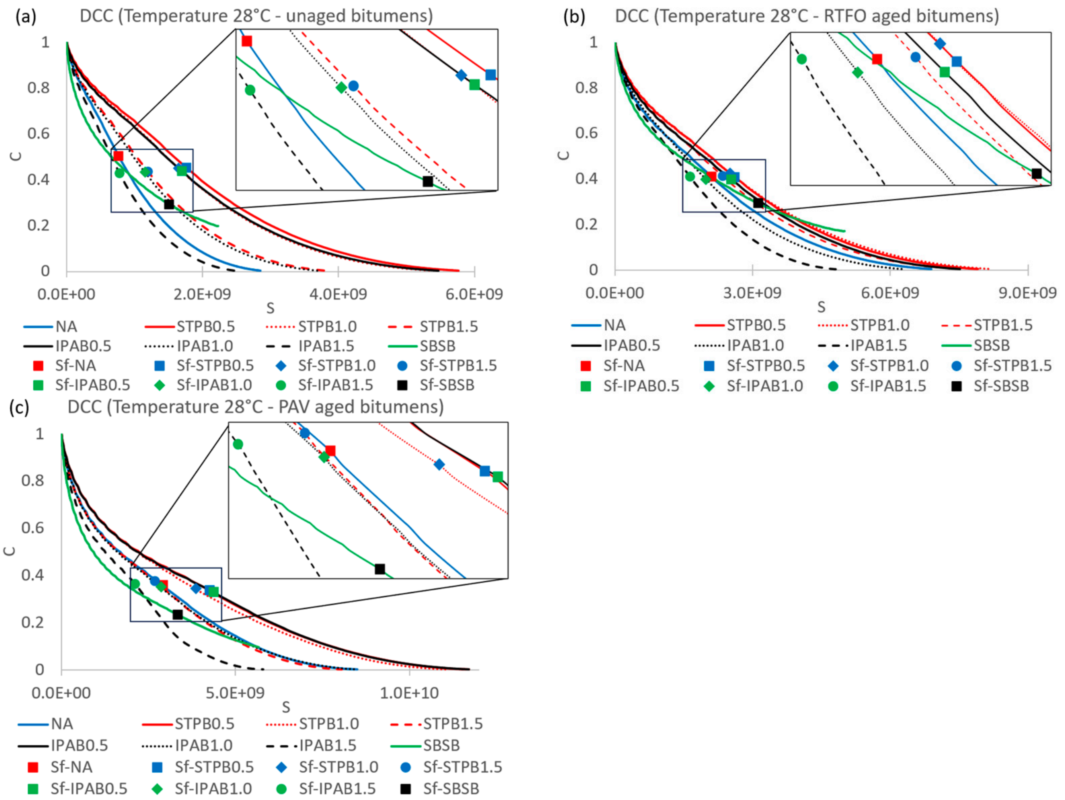

Figure 16. The DCCs with failure points identified using the peak of SPC at 28 °C: (**a**) unaged bitumens; (**b**) RTFO-aged bitumens; and (**c**) PAV-aged bitumens.

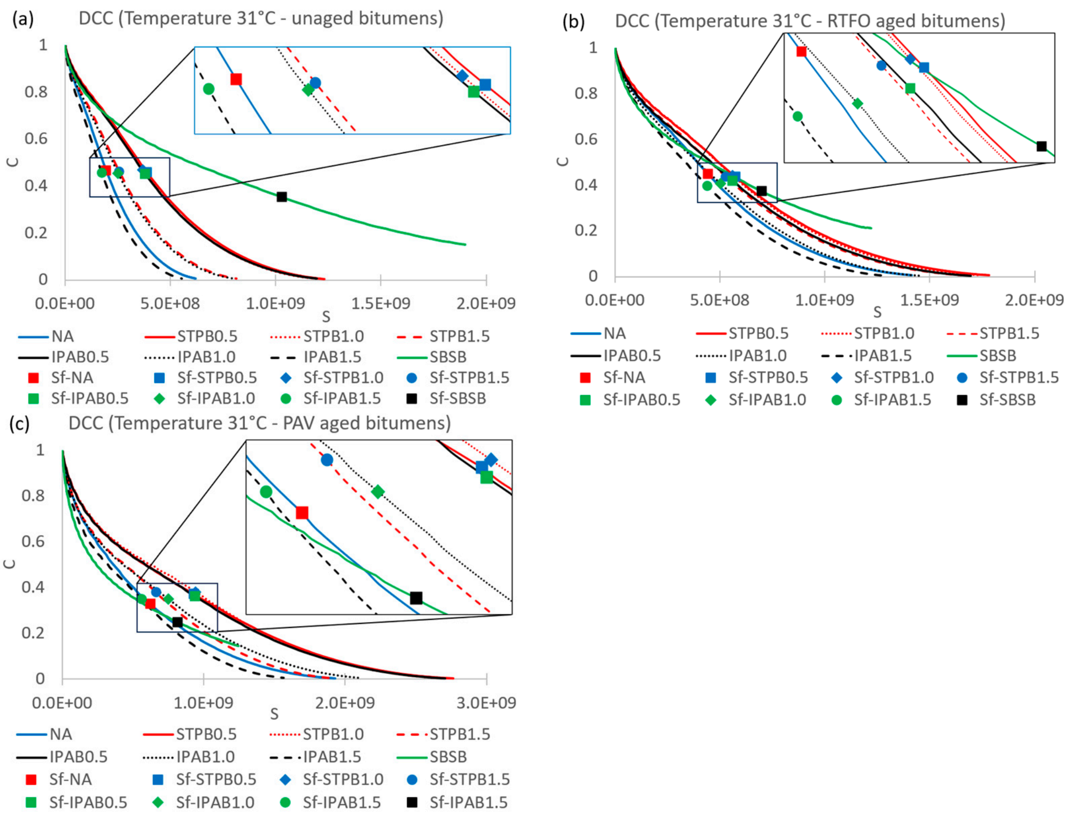

Figure 17. The DCCs with failure points identified using the peak of SPC at 31 °C: (**a**) unaged bitumens; (**b**) RTFO-aged bitumens; and (**c**) PAV-aged bitumens.

Figure 17a,b show the SBSB with higher S_f than the other bitumens. In the case of Figure 17a, SBSB exhibited greater fatigue performance in terms of C values regardless of the S values, and this was because its corresponding DCC was generally over the other DCCs in the abovementioned figure section. Hence, in Figure 17a, the bitumen with higher S_f also exhibited the best fatigue behavior. However, in Figure 17b, even though the SBSB displayed the DCC with a greater S_f than the other asphalt binders in this figure section, it was not clear whether SBSB showed a superior fatigue performance concerning the other bitumens in terms of the C values (regardless of S values). This was because the DCC linked with SBSB was usually below the DCCs related to STPB0.5 and STPB1.0 up to the SBSB failure point.

Figure S11g,h depict the SPC and RPC curves associated with Figures 17a and 17b, respectively. In the case of Figure S11g, SBSB exhibited the SPC curve with a higher S_f and fatigue performance than the other bitumens in this study because its SPC curve had its peak at the right side of the other SPC curve peaks and was mainly above the other curves related to the other asphalt binders. In Figure S11h, the SPC curve associated with SBSB showed the greatest S_f because its SPC curve peak was located at the right side concerning the other SPC curve peaks. Nevertheless, in this figure section, the SPC curve linked with SBSB was generally below the SPC curves associated with STPB0.5 and STPB1.0 up to the peak of the SPC curve linked with SBSB. As a result, it was not clear whether SBSB showed a superior fatigue performance or not. The findings from Figure 17a,b and Figure S11g,h are aligned. Hence, it can be concluded that a bitumen with a higher S_f does not always exhibit greater fatigue performance.

To clarify whether or not SBSB exhibits superior fatigue performance in the abovementioned cases, the CW concept was used. Tables S1, S5, S9, S13, S17, S21, S25, S29 and S33 (see Supplementary Materials) show the CW_{DCC} values at different temperature and aging conditions. Tables S2, S6, S10, S14, S18, S22, S26, S30 and S34 (see Supplementary Materials) show the CW_{SPC} values at different temperature and aging conditions. Tables S3, S7, S11, S15, S19, S23, S27, S31 and S35 (see Supplementary Materials) show the ranking related to the CW_{DCC} values at different temperature and aging conditions with respect to each failure point. Tables S4, S8, S12, S16, S20, S24, S28, S32 and S36 (see Supplementary Materials) show the ranking related to the CW_{SPC} values at different temperature and aging conditions with respect to each failure point. CW_{DCC} and CW_{SPC} are the parameters proposed in this study to precisely assess the bitumen fatigue performance considering the C-S values and SPC-S values.

After comprehensively analyzing all the values from the abovementioned tables, as well as Figure 15, Figure 16, Figure 17 and Figure S11, it can be concluded that CW_{DCC} and CW_{SPC} can be used to accurately evaluate the asphalt binder fatigue performance in the C vs. S and SPC vs. S graphs, respectively. Moreover, CW_{DCC} and CW_{SPC} establish a strong correlation between the C vs. S and SPC vs. S graphs because the rankings of the bitumen fatigue performances in the former graph were the same as the rankings related to the asphalt binder fatigue behavior in the latter graph. As a result, the inconsistency between the failure definition and the fatigue performance related to the DCC in ranking a group of bitumens in terms of fatigue behavior was solved, at least for the asphalt binders and test conditions selected in this study.

3.4. Failure Criterion Evaluation (Proposal)

Figures 18 and 19 represent the new proposal of a failure criterion related to RTFO-aged and PAV-aged bitumens, respectively. Figure 18 is associated with the following test sets: 2a, 3a, 4a, 5a, 6a, 7a, 8a, and 9a. Figure 19 is linked with the test sets 2b, 3b, 4b, 5b, 6b, 7b, 8b, and 9b. Figures 18 and 19 exhibit strong relationships between C^R and S_f, regardless of the bitumens and experimental conditions, and this was because the R^2 values were always greater than 0.90. Hence, it is possible to confirm that the failure criterion based on the sum of all RPC values up to the failure point defined by S_f can be used to accurately predict the fatigue performance of asphalt binders under different test conditions, at least for those selected in this study. Furthermore, the slopes of the fitting graphs shown in Figures 18 and 19 are generally quite similar, which means that the new proposal of a failure criterion identifies a similar tendency as to the change in the average rate of released potential cohesion during the cLAS test. Moreover, this proves that the bitumen aging condition had a low influence on how the C^R values changed, at least for the bitumens selected in this study. Concluding this section, we can confirm that the new failure criterion proposal solved the inadequacy identified in the previous failure criterion.

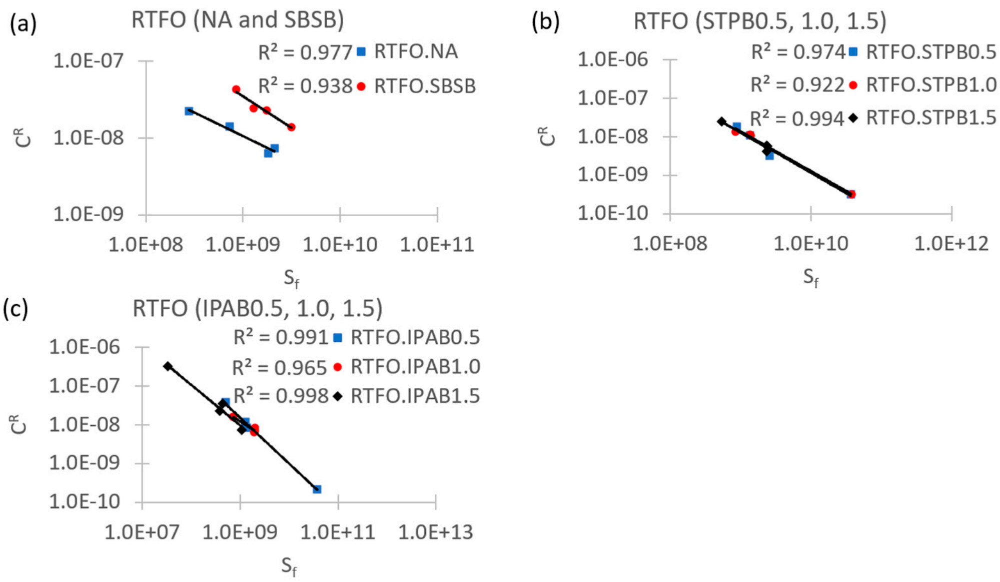

Figure 18. C^R vs. S_f graph of the RTFO-aged bitumens: (**a**) NA and SBSB; (**b**) STPB 0.5-1.0-1.5; and (**c**) IPAB 0.5-1.0-1.5.

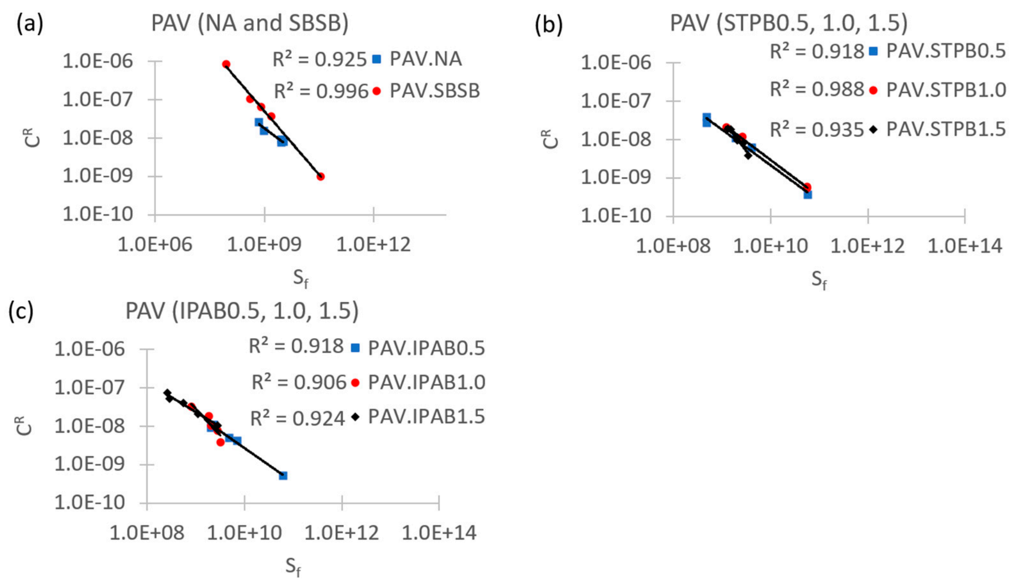

Figure 19. C^R vs. S_f graph of the PAV-aged bitumens: (**a**) NA and SBSB; (**b**) STPB 0.5-1.0-1.5; and (**c**) IPAB 0.5-1.0-1.5.

4. Discussion

In Section 3.1, the current framework showed that asphalt binders with a greater number of loading cycles required to reach their failure points (N_f) failed to exhibit superior fatigue performances in terms of the DCC evaluation. This finding aligned with previous research works, such as in—for instance—Wang et al. [9] and Lv et al. [23], and this also proved the need for a new failure definition. This fact demonstrated the ranking inconsistency between the traditional failure definition (stored PSE peak) and the fatigue behavior according to DCC interpretation under the current framework. As a result, there was a necessity to introduce a developed framework (failure definition) based on "S" instead of N to fix the abovementioned inadequacy. After conducting a comprehensive analysis of previous failure definitions, this research team realized that most of them include the parameter "C" because material integrity has a high influence on bitumen fatigue response.

Furthermore, previous failure definitions are mainly based on the number of loading cycles; however, each loading cycle has a different effect on bitumen fatigue behavior, which can be one of the reasons for introducing uncertainties (as mentioned above) into the failure definition under certain conditions. One method of identifying the effect of each loading cycle on asphalt binder fatigue behavior is to analyze the damage intensity at each loading cycle. As a result, this research team developed the framework, utilizing "S" instead of "N", to determine the failure definition and to increase the efficiency with respect to the current framework. Hence, the developed failure definition concept proposed in this study solved the ranking inconsistency of fatigue performance between the failure definition and DCC evaluation.

According to the DCC assessment, the developed and current frameworks showed that SBSB generally shows lower fatigue behavior than the other bitumens analyzed in this study. This phenomenon also occurred in previous studies, such as in—for instance—Safaei et al. [3], Wang et al. [8], and Wang et al. [9]; however, these results were not aligned with the practical use of SBSB in road construction. Additionally, the developed and current frameworks showed that PAV-aged bitumens generally display superior fatigue performance over RTFO-aged asphalt binders and unaged bitumens in terms of the DCC evaluation. This finding conflicts with the actual engineering experience, but it agrees with previous studies, such as in—for instance—Chen and Bahia [49], Cao and Wang [14], and Zhou et al. [21]. It is necessary to point out that both previous inadequacies (related to SBSB and PAV-aged bitumens) demonstrate that the proposed framework needs further development to fix the two abovementioned inconsistencies. Although this study found these issues in the developed and current frameworks, their solutions were beyond the focus of this research. The main objective of this study was to solve the ranking inconsistency between the failure definition and DCC analysis of the current framework. This scenario led to our expectation of some modifications to the S-VECD model's formulation in determining C and S values in the near future. However, the developed framework (failure definition) should continue to be effective in identifying the failure point because it is based on the calculated C and S values and not on the equation used to determine those parameters. Another contribution of this research work was that the newly proposed failure definition could find the failure point in some cases where the previous failure definition could not identify the fatigue life because the stored PSE curve lacks a peak (i.e., always increases).

It is noteworthy that both frameworks tested in this study identified that almost all bitumens exhibited their best fatigue performances at 28 °C in terms of DCC evaluation regardless of aging condition. This phenomenon led us to infer that there might be a temperature at which each asphalt binder shows its best fatigue performance in terms of the DCC interpretation. This finding conflicted with the previous research of Wang et al. [9] and aligned with Chen et al. [25] in terms of TTSP. This research team considers that, after a comprehensive analysis, the main contribution of this finding (in this study) was in providing a possible explanation for the previous phenomenon (i.e., that TTSP is not always applicable). As a result, it is possible that both studies were right because the TTSP should be applicable at a temperature range that is lower or higher than the specific temperature that causes the best bitumen fatigue performance in terms of the DCC assessment, and this is because this specific temperature should change the movement tendency of DCCs when increasing or decreasing the test temperature. However, more experimental tests are needed to prove this theory.

The current framework (failure criterion), which is based on the TRPSE in terms of the area under the released PSE curve up to the failure point, failed to predict the bitumen fatigue performance under any type of condition because the R^2 values were low in some cases. Although the stored PSE is a suitable tool for evaluating bitumen capacity to store more energy in the form of loading amplitude (energy input), when conducting the cLAS under certain conditions, it failed to identify the bitumen failure point, as mentioned before. This introduced some uncertainties in the current framework (failure criterion), which caused low R^2 values in some specific cases. Hence, another contribution of this study was that the developed framework (the proposed failure criterion) solved this problem because it included a failure definition that was able to identify the failure points where the current failure definition could not. As a result, the proposed failure criterion, which is based on the sum of all RPC values up to the failure point defined by S_f, accurately predicted the fatigue performance of the asphalt binders under different test conditions, at least for those selected in this study.

As mentioned before, a framework that evaluates bitumen fatigue performance should include three elements: the linear viscoelastic (LVE) responses, DCC properties, and the failure criterion determination [9]. The framework developed in this study (i.e., the new failure definition and failure criterion) included all the elements defined by C. Wang et al. [9], and it utilized them in the process to rank the fatigue performance of a group of asphalt binders. This developed procedure consistently identified STPB0.5, STPB1.0, and IPAB0.5 as the top (in rank) three asphalt binders according to the CW_{DCC} (see Tables S11, S23 and S35) and CW_{SPC} (see Tables S12, S24 and S36) regardless of the temperature. The identified rankings are consistent with respect to both groups of tables. Our research team considers that the developed framework overcomes the inconsistency of the current framework because it is mainly based on "S" instead of "N". Moreover, the SPC (which includes C and S values) is a parameter that follows the exact shape of the DCC and represents the real bitumen fatigue stage at the decided point in the DCC. This ensures a precise analysis of the bitumen fatigue performance.

The developed framework (the proposed failure criterion) identified similar slopes of the fitting graphs related to all of the PAV-aged bitumens (see Figure S12). This means that the proposed failure criterion identified comparable tendencies of how the average rate of the RPC changes while conducting the cLAS test. In the newly proposed procedure, the steeper and flatter fitting graph slopes indicated that the bitumen loses the capacity to maintain as high an integrity as possible at faster and slower rates, respectively. With regard to all the bitumens, SBSB and STPB0.5 showed the highest and lowest average rates of RPC in this study.

In the developed framework, the sum of rankings of all the PAV-aged bitumens related to the failure definition (based on the CW_{DCC} and CW_{SPC}) and failure criterion were obtained and are shown in Table 7. By conducting this process, the developed framework presented a general overview regarding the bitumen fatigue performance considering the (LVE) responses, DCC properties, and failure criterion determination, as defined by C. Wang et al. [9]. This fact represents the superiority of the developed framework with respect to previous frameworks because only one parameter (sum of rankings) provided a general view of bitumen fatigue performance considering (LVE) responses, DCC properties, and failure criterion determination at the same time. Hence, the proposed procedure can be used to determine the bitumen with the best performance. Bitumens with the lowest and the highest sum of rankings exhibited the greatest and the poorest fatigue performance according to the abovementioned parameters, respectively. As a result, the developed framework identified that PAV-STPB0.5 and PAV-SBSB exhibited the lowest and the highest sum of rankings, respectively (see Table 7). This meant that, according to the proposed procedure, the former showed the best, and the latter exhibited the poorest fatigue cracking performance among all the bitumens in this study.

Table 7. Sum of the rankings of the PAV-aged bitumens (STPB0.5, STPB1.0, and IPAB0.5).

Bitumen	Ranking of CW_{DCC} and CW_{SPC}			Ranking of C^R	Sum of Rankings
	T (25 °C)	T (28 °C)	T (31 °C)		
PAV-NA	6	4	6	2	18
PAV-STPB0.5	3	1	2	1	7
PAV-STPB1.0	1	3	1	6	11
PAV-STPB1.5	4	5	5	3	17
PAV-IPAB0.5	2	2	3	5	12
PAV-IPAB1.0	5	6	4	4	16
PAV-IPAB1.5	7	7	7	7	28
PAV-SBSB	8	8	8	8	32

Future research will focus on improving the developed framework to address the abovementioned inconsistency between SBSB fatigue cracking performance (in terms of DCC analysis) and the practical engineering use of SBSB in road construction. Another focus of future studies will be in enhancing the proposed procedure for addressing the inadequacy between the fatigue cracking performance of PAV-aged bitumens and the behavior of asphalt binders with less aging, and this will be performed because the former group of bitumens showed superior fatigue performance over the latter group in terms of DCC assessment, which does not align with the practical experience in road construction. In addition, future research will investigate the existence of a specific temperature (different from one asphalt binder to another), which will ensure the best fatigue cracking performance of each bitumen in terms of DCC analysis according to the findings in this study. Additionally, the capacity of the framework developed in this research in assessing the self-restoration performance of different types of asphalt binders will be evaluated.

5. Conclusions

In this research, the capacities of the newly proposed and current frameworks in accommodating the bitumen fatigue cracking performance were evaluated. Both frameworks were based on the LAS test and the S-VECD model. The main issue addressed in this study was the ranking inconsistency between the failure definition and DCC analysis. Eight different bitumens were tested to assess the usefulness of the abovementioned frameworks. After comprehensively evaluating the experimental results, the following conclusions could be drawn:

- Bitumens with a higherN_f failed to show greater fatigue performance in terms of the DCC analysis, which confirmed the ranking inconsistency between the failure definition and DCC assessment included in the current framework in terms of evaluating bitumen fatigue cracking performance.
- The developed framework being based on "S" instead of "N" eliminated the ranking inconsistency between the failure definition and DCC analysis.
- The PAV-aged bitumens generally exhibited superior fatigue performance over the RTFO-aged asphalt binders and unaged bitumens in terms of the DCC assessment, which conflicts with actual engineering experience.
- In some cases, determining the bitumen failure point by utilizing the current framework was impossible because the stored PSE curve lacked a peak. This issue was solved utilizing the developed framework.
- The bitumens in this study mostly exhibited their best fatigue performance at 28 °C in terms of DCC analysis regardless of the aging conditions. This phenomenon led to the inference that there might be a temperature at which each asphalt binder exhibits its best performance in terms of the DCC assessment.
- The failure criterion (current framework) based on the TRPSE was not useful in predicting bitumen fatigue performance under any condition because sometimes the R^2 values were below 0.9 and even lower than 0.1. This issue was solved utilizing the developed framework.

- According to the developed framework, the bitumen that showed the best fatigue performance based on the LVE responses, DCC properties, and failure criterion determination was STPB0.5.

6. Recommendations

The recommendations in this study are as follows:

- Try to determine the equation that best fits modeling the DCC and SPC to ensure a high-quality analysis of the bitumen fatigue performance by utilizing the developed framework.
- Evaluate the developed framework's capacity to accommodate the fatigue performance of other types of asphalt binder under different test conditions.
- Assess the developed framework's capacity to accommodate the fatigue performance of asphalt mixtures.
- Improve the formulation of the developed framework to address the remaining inconsistency in bitumen fatigue performance analysis (e.g., PAV-aged bitumens generally exhibit superior fatigue performance over RTFO-aged asphalt binders and unaged bitumens in terms of DCC assessment, and SBSB generally shows lower fatigue behavior than the other bitumens in this study according to the DCC assessment). These phenomena conflict with the actual engineering experience.

Supplementary Materials: The following supporting information can be downloaded at: https://www.mdpi.com/article/10.3390/buildings14020311/s1, Figure S1: Stored PSE curves of the bitumens at different temperature and aging conditions: (a) T25 °C—unaged; (b) T25 °C—RTFO-aged; (c) T25 °C—PAV-aged; (d) T28 °C—unaged; (e) T28 °C—RTFO-aged; (f) T28 °C—PAV-aged; (g) T31 °C—unaged; (h) T31 °C—RTFO-aged; and (i) T31 °C—PAV-aged. Figure S2: DCCs of the NA at different temperature and aging conditions: (a) unaged NA—T25, T28, and T31; (b) RTFO-aged NA—T25, T28, and T31; (c) PAV-aged NA—T25, T28, and T31; (d) T25—unaged NA, RTFO-aged NA, and PAV-aged NA; (e) T28—unaged NA, RTFO-aged NA, and PAV-aged NA; and (f) T31—unaged NA, RTFO-aged NA, and PAV-aged NA. Figure S3: DCCs of STPB0.5 at different temperature and aging conditions: (a) unaged STPB0.5—T25, T28, and T31; (b) RTFO-aged STPB0.5—T25, T28, and T31; (c) PAV-aged STPB0.5—T25, T28, and T31; (d) T25—unaged STPB0.5, RTFO-aged STPB0.5, and PAV-aged STPB0.5; (e) T28—unaged STPB0.5, RTFO-aged STPB0.5, and PAV-aged STPB0.5; and (f) T31—unaged STPB0.5, RTFO-aged STPB0.5, and PAV-aged STPB0.5. Figure S4: DCCs of STPB1.0 at different temperature and aging conditions: (a) unaged STPB1.0—T25, T28, and T31; (b) RTFO-aged STPB1.0—T25, T28, and T31; (c) PAV-aged STPB1.0—T25, T28, and T31; (d) T25—unaged STPB1.0, RTFO-aged STPB1.0, and PAV-aged STPB1.0; (e) T28—unaged STPB1.0, RTFO-aged STPB1.0, and PAV-aged STPB1.0; and (f) T31—unaged STPB1.0, RTFO-aged STPB1.0, and PAV-aged STPB1.0. Figure S5: DCCs of STPB1.5 at different temperature and aging conditions: a) unaged STPB1.5—T25, T28, and T31; (b) RTFO-aged STPB1.5—T25, T28, and T31; (c) PAV-aged STPB1.5—T25, T28, and T31; (d) T25—unaged STPB1.5, RTFO-aged STPB1.5, and PAV-aged STPB1.5; (e) T28—unaged STPB1.5, RTFO-aged STPB1.5, and PAV-aged STPB1.5; (f) T31—unaged STPB1.5, RTFO-aged STPB1.5, and PAV-aged STPB1.5. Figure S6: DCCs of IPAB0.5 at different temperature and aging conditions: a) unaged IPAB0.5—T25, T28, and T31; (b) RTFO-aged IPAB0.5—T25, T28, and T31; (c) PAV-aged IPAB0.5—T25, T28, and T31; (d) T25—unaged IPAB0.5, RTFO-aged IPAB0.5, and PAV-aged IPAB0.5; (e) T28—unaged IPAB0.5, RTFO-aged IPAB0.5, and PAV-aged IPAB0.5; and (f) T31—unaged IPAB0.5, RTFO-aged IPAB0.5, and PAV-aged IPAB0.5. Figure S7: DCCs of IPAB1.0 at different temperature and aging conditions: a) unaged IPAB1.0—T25, T28, and T31; (b) RTFO-aged IPAB1.0—T25, T28, and T31; (c) PAV-aged IPAB1.0—T25, T28, and T31; (d) T25—unaged IPAB1.0, RTFO-aged IPAB1.0, and PAV-aged IPAB1.0; (e) T28—unaged IPAB1.0, RTFO-aged IPAB1.0, and PAV-aged IPAB1.0; and (f) T31—unaged IPAB1.0, RTFO-aged IPAB1.0, and PAV-aged IPAB1.0. Figure S8: DCCs of IPAB1.5 at different temperature and aging conditions: a) unaged IPAB1.5—T25, T28, and T31; (b) RTFO-aged IPAB1.5—T25, T28, and T31; (c) PAV-aged IPAB1.5—T25, T28, and T31; (d) T25—unaged IPAB1.5, RTFO-aged IPAB1.5, and PAV-aged IPAB1.5; (e) T28—unaged IPAB1.5, RTFO-aged IPAB1.5, and PAV-aged IPAB1.5; and (f) T31—unaged IPAB1.5, RTFO-aged IPAB1.5, and PAV-aged IPAB1.5. Figure S9: DCCs of SBSB at different temperature and aging conditions: a) unaged SBSB—T25, T28, and T31; (b) RTFO-aged SBSB—T25, T28, and T31; (c) PAV-aged SBSB—T25, T28, and T31; (d) T25—unaged SBSB, RTFO-aged SBSB, and PAV-aged SBSB; (e) T28—unaged SBSB, RTFO-aged SBSB, and PAV-aged SBSB; (f) T31—unaged SBSB, RTFO-aged SBSB, and PAV-aged SBSB. Figure S10: Failure definition points identified by the peak of W^R (N_f) and the peak of SPC (S_f) on the W^R curve: (a) T 25 °C—unaged bitumens, (a-1) zoom (peaks of PSE curves in (a)); (b) T 25 °C—RTFO-aged bitumens, (b-1) zoom (peaks of PSE curves in (b)); (c) T 25 °C—PAV-aged bitumens, (c-1) zoom (peaks of PSE curves in (c)); (d) T 28 °C—unaged bitumens, (d-1) zoom (peaks of PSE curves in (d)); (e) T 28 °C—RTFO-aged bitumens, (e-1) zoom (peaks of PSE curves in (e)); (f) T 28 °C—PAV-aged bitumens, (f-1) zoom (peaks of PSE curves in (f)); (g) T 31 °C—unaged bitumens, (g-1) zoom (peaks of PSE curves in (g)); (h) T 31 °C—RTFO-aged bitumens, (h-1) zoom (peaks of PSE curves in (h)); and (i) T 31 °C—PAV-aged bitumens, (i-1) zoom (peaks of PSE curves in (i)). Figure S11: SPC and RPC curves of bitumens: (a) T 25 °C—unaged bitumens; (b) T 25 °C—RTFO-aged bitumens; (c) T 25 °C—PAV-aged bitumens; (d) T 28 °C—unaged bitumens; (e) T 28 °C—RTFO-aged bitumens; (f) T 28 °C—PAV-aged bitumens; (g) T 31 °C—unaged bitumens; (h) T 31 °C—RTFO-aged bitumens; and (i) T 31 °C—PAV-aged bitumens. Figure S12: C^R vs. S_f graph of all PAV-aged bitumens. Table S1: CW_{DCC} of unaged bitumens at each failure point (25 °C). Table S2: CW_{SPC} of unaged bitumens at each failure point (25 °C). Table S3: Ranking of the CW_{DCC} of unaged bitumens with respect to each failure point (25 °C). Table S4: Ranking of the CW_{SPC} of unaged bitumens with respect to each failure point (25 °C). Table S5: CW_{DCC} of RTFO-aged bitumens at each failure point (25 °C). Table S6: CW_{SPC} of RTFO-aged bitumens at each failure point (25 °C). Table S7: Ranking of the CW_{DCC} of RTFO-aged bitumens with respect to each failure point (25 °C). Table S8: Ranking of the CW_{SPC} of RTFO-aged bitumens with respect to each failure point (25 °C). Table S9: CW_{DCC} of the PAV-aged bitumens at each failure point (25 °C). Table S10: CW_{SPC} of the PAV-aged bitumens at each failure point (25 °C). Table S11: Ranking of the CW_{DCC} of PAV-aged bitumens with respect to each failure point (25 °C). Table S12: Ranking of the CW_{SPC} of PAV-aged bitumens with respect to each failure point (25 °C). Table S13: CW_{DCC} of unaged bitumens at each failure point (28 °C). Table S14: CW_{SPC} of unaged bitumens at each failure point (28 °C). Table S15: Ranking of the CW_{DCC} of unaged bitumens with respect to each failure point (28 °C). Table S16: Ranking of the CW_{SPC} of unaged bitumens with respect to each failure point (28 °C). Table S17: CW_{DCC} of the RTFO-aged bitumens at each failure point (28 °C). Table S18: CW_{SPC} of the RTFO-aged bitumens at each failure point (28 °C). Table S19: Ranking of the CW_{DCC} of RTFO-aged bitumens with respect to each failure point (28 °C). Table S20: Ranking of the CW_{SPC} of RTFO-aged bitumens with respect to each failure point (28 °C). Table S21: CW_{DCC} of PAV-aged bitumens at each failure point (28 °C). Table S22: CW_{SPC} of PAV-aged bitumens at each failure point (28 °C). Table S23: Ranking of the CW_{DCC} of PAV-aged bitumens with respect to each failure point (28 °C). Table S24: Ranking of the CW_{SPC} of PAV-aged bitumens with respect to each failure point (28 °C). Table S25: CW_{DCC} of unaged bitumens at each failure point (31 °C). Table S26: CW_{SPC} of unaged bitumens at each failure point (31 °C). Table S27: Ranking of the CW_{DCC} of unaged bitumens with respect to each failure point (31 °C). Table S28: Ranking of the CW_{SPC} of unaged bitumens with respect to each failure point (31 °C). Table S29: CW_{DCC} of RTFO-aged bitumens at each failure point (31 °C). Table S30: CW_{SPC} of RTFO-aged bitumens at each failure point (31 °C). Table S31: Ranking of the CW_{DCC} of RTFO-aged bitumens with respect to each failure point (31 °C). Table S32: Ranking of the CW_{SPC} of RTFO-aged bitumens with respect to each failure point (31 °C). Table S33: CW_{DCC} of PAV-aged bitumens at each failure point (31 °C). Table S34: CW_{SPC} of PAV-aged bitumens at each failure point (31 °C). Table S35: Ranking of the CW_{DCC} of PAV-aged bitumens with respect to each failure point (31 °C). Table S36: Ranking of the CW_{SPC} of PAV-aged bitumens with respect to each failure point (31 °C).

Author Contributions: Conceptualization, S.L., D.G. and M.B.C.; methodology, M.B.C.; software, M.B.C., validation, M.B.C., formal analysis, M.B.C.; investigation, S.C., D.L. and W.Z.; resources, S.L., D.G., C.-H.L. and M.B.C.; data curation, M.B.C.; writing—original draft preparation, M.B.C. and C.L; writing—review and editing, M.B.C. and C.-H.L.; visualization, S.L., D.G. and M.B.C.; supervision, S.L., D.G. and M.B.C.; project administration, S.L., D.G. and M.B.C.; funding acquisition, S.L., D.G., C.-H.L. and M.B.C. All authors have read and agreed to the published version of the manuscript.

Funding: This research was funded by the Key Laboratory of Road Structure and Material of Ministry of Transport (Changsha), Changsha University of Science & Technology, grant number kfj220305.

Data Availability Statement: Data are contained within the article.

Conflicts of Interest: The authors declare no conflicts of interest.

References

1. Zeiada, W.A.; Souliman, M.I.; Kaloush, K.E.; Mamlouk, M.; Underwood, B.S. Comparison of fatigue damage, healing, and endurance limit with beam and uniaxial fatigue tests. *Transp. Res. Rec.* **2014**, *2447*, 32–41. [CrossRef]
2. Motamed, A.; Bhasin, A.; Izadi, A. Evaluating Fatigue-Cracking Resistance of Asphalt Binders in a Standardized Composite Using Continuum Damage Theory. *J. Mater. Civ. Eng.* **2013**, *25*, 1209–1219. [CrossRef]
3. Safaei, F.; Castorena, C.; Kim, Y.R. Linking asphalt binder fatigue to asphalt mixture fatigue performance using viscoelastic continuum damage modeling. *Mech. Time-Depend. Mater.* **2016**, *20*, 299–323. [CrossRef]
4. Zhang, Z.; Oeser, M. Energy dissipation and rheological property degradation of asphalt binder under repeated shearing with different oscillation amplitudes. *Int. J. Fatigue* **2021**, *152*, 106417. [CrossRef]
5. *AASHTO TP 101-14*; Estimating Damage Tolerance of Asphalt Binders Using the Linear Amplitude Sweep. American Association of State Highway and Transportation Officials: Washington, DC, USA, 2014.
6. Hintz, C.; Bahia, H. Simplification of Linear Amplitude Sweep Test and Specification Parameter. *Transp. Res. Rec.* **2013**, *2370*, 10–16. [CrossRef]
7. Hintz, C.; Velasquez, R.; Johnson, C.; Bahia, H. Modification and validation of linear amplitude sweep test for binder fatigue specification. *Transp. Res. Rec.* **2011**, *2207*, 99–106. [CrossRef]
8. Wang, C.; Castorena, C.; Zhang, J.; Kim, Y.R. Unified failure criterion for asphalt binder under cyclic fatigue loading. *Road Mater. Pavement Des.* **2015**, *16*, 125–148. [CrossRef]
9. Wang, C.; Castrorena, C.; Zhang, J.; Kim, Y.R. Application of Time-Temperature Superposition Principle on Fatigue Failure Analysis of Asphalt Binder. *J. Mater. Civ. Eng.* **2017**, *29*, 04016194. [CrossRef]
10. Ameri, M.; Mansourkhaki, A.; Daryaee, D. Evaluation of fatigue behavior of asphalt binders containing reclaimed asphalt binder using simplified viscoelastic continuum damage approach. *Constr. Build. Mater.* **2019**, *202*, 374–386. [CrossRef]
11. Roque, R.; Yan, Y.; Lopp, G. *Cracking Performance Evaluation of Asphalt Binders At Intermediate Temperature*; Contract No. BDV31-977-83. Final Report; University of Florida and Florida Department of Transportation: Gainesville, FL, USA, 2020.
12. Schapery, R.A. Correspondence principles and a generalized J integral for large deformation and fracture analysis of viscoelastic media. *Int. J. Fract.* **1984**, *25*, 195–223. [CrossRef]
13. Park, S.W.; Kim, Y.R.; Schapery, R.A. A viscoelastic continuum damage model and its application to uniaxial behavior of asphalt concrete. *Mech. Mater.* **1996**, *24*, 241–255. [CrossRef]
14. Cao, W.; Wang, C. A new comprehensive analysis framework for fatigue characterization of asphalt binder using the Linear Amplitude Sweep test. *Constr. Build. Mater.* **2018**, *171*, 1–12. [CrossRef]
15. Moreno-Navarro, F.; Ayar, P.; Sol-Sánchez, M.; Rubio-Gámez, M.C. Exploring the recovery of fatigue damage in bituminous mixtures at macro-crack level: The influence of temperature, time, and external loads. *Road Mater. Pavement Des.* **2017**, *18*, 293–303. [CrossRef]
16. Babadopulos, L.F.D.A.L.; Orozco, G.; Sauzéat, C.; Di Benedetto, H. Reversible phenomena and fatigue damage during cyclic loading and rest periods on bitumen. *Int. J. Fatigue* **2019**, *124*, 303–314. [CrossRef]
17. Safaei, F.; Lee, J.; Nascimento, L.A.H.D.; Hintz, C.; Kim, Y.R. Implications of Warm-Mix asphalt on long term oxidative aging and fatigue performance of asphalt binders and mixtures. *Road Mater. Pavement Des.* **2014**, *15*, 45–61. [CrossRef]
18. Reese, R. Properties of aged asphalt binder related to asphalt concrete fatigue life. *J. Assoc. Asph. Paving Technol.* **1997**, *66*, 604–632.
19. Masad, E.; Branco, V.T.F.C.; Little, D.N.; Lytton, R. A unified method for the analysis of controlled-strain and controlled-stress fatigue testing. *Int. J. Pavement Eng.* **2008**, *9*, 233–246. [CrossRef]
20. Sabouri, M.; Kim, Y.R. Development of a failure criterion for asphalt mixtures under different modes of fatigue loading. *Transp. Res. Rec.* **2014**, *2447*, 117–125. [CrossRef]
21. Zhou, F.; Karki, P.; Im, S. Development of a Simple Fatigue Cracking Test for Asphalt Binders. *Transp. Res. Rec. J. Ofthe Transp. Res. Board* **2017**, *2632*, 79–87. [CrossRef]
22. Zhang, R.; Sias, J.E.; Dave, E.V. Development of new performance indices to evaluate the fatigue properties of asphalt binders with ageing. *Road Mater. Pavement Des.* **2020**, *23*, 377–396. [CrossRef]
23. Lv, S.; Ge, D.; Wang, Z.; Wang, J.; Liu, J.; Ju, Z.; Peng, X.; Fan, X.; Cao, S.; Liu, D.; et al. Performance Assessment of Self-Healing Polymer-Modified Bitumens by Evaluating the Suitability of Current Failure Definition. *Fail. Criterion Fatigue-Restor. Criteria Mater.* **2023**, *16*, 2488. [CrossRef]
24. Ilyin, S.O.; Yadykova, A.Y. Eco-friendly bitumen binders from heavy crude oil and a relaxation approach to predicting their resistance to rutting and cracking. *J. Clean. Prod.* **2024**, *434*, 139942. [CrossRef]
25. Chen, H.; Zhang, Y.; Bahia, H.U. Estimating asphalt binder fatigue at multiple temperatures using a simplified pseudo-strain energy analysis approach in the LAS test. *Constr. Build. Mater.* **2021**, *266*, 120911. [CrossRef]
26. Safaei, F.; Castorena, C. Temperature effects of linear amplitude sweep testing and analysis. *Transp. Res. Rec.* **2016**, *2574*, 92–100. [CrossRef]
27. Wang, C.; Xie, W.; Chen, Y.; Diab, A.; You, Z. Refining the Calculation Method for Fatigue Failure Criterion of Asphalt Binder from Linear Amplitude Sweep Test. *J. Mater. Civ. Eng.* **2018**, *30*, 04017286. [CrossRef]

28. Sun, G.; Ma, J.; Sun, D.; Li, B.; Ling, S.; Lu, T. Influence of thermal oxidative aging on temperature induced self-healing transition of polymer modified bitumens. *Mater. Des.* **2020**, *192*, 108717. [CrossRef]
29. Zhang, T.; Gao, S.; Yu, J.; He, Y.; Han, X.; Zhuang, R. Preparation and performance of self-healing SBS modified bitumen based on dynamic disulfide bonds. *Constr. Build. Mater.* **2023**, *397*, 132394. [CrossRef]
30. Yousif, R.A.; Tayh, S.A.; Al-Saadi, I.F.; Jasim, A.F. Physical and Rheological Properties of Asphalt Binder Modified with Recycled Fibers. *Adv. Civ. Eng.* **2022**, *2022*, 1223467. [CrossRef]
31. Kök, B.V.; Çolak, H. Laboratory comparison of the crumb-rubber and SBS modified bitumen and hot mix asphalt. *Constr. Build. Mater.* **2011**, *25*, 3204–3212. [CrossRef]
32. Sun, P.; Zhang, K.; Xiao, Y.; Liang, Z. Analysis of Pavement Performance for Nano-CaCO3/SBS Modified Asphalt Mixture. *J. Phys. Conf. Ser.* **2022**, *2329*, 012031. [CrossRef]
33. Li, X.; Guo, D.; Xu, M.; Guo, C.; Wang, D. REOB/SBS Composite-Modified Bitumen Preparation and Modification Mechanism Analysis. *Buildings* **2023**, *13*, 1601. [CrossRef]
34. Zhang, W.; Zou, L.; Chen, F.; Yang, C.; Li, Y.; Yan, X.; Zang, J.; Liu, J. Evaluation method of storage stability of SBS modified bitumen based on dynamic rheological properties. *Constr. Build. Mater.* **2022**, *323*, 126615. [CrossRef]
35. Li, Y.; Li, W.; Sun, A.; Jing, M.; Liu, X.; Wei, L.; Wu, K.; Fu, Q. A self-reinforcing and self-healing elastomer with high strength, unprecedented toughness and room-temperature reparability. *Mater. Horiz.* **2020**, *8*, 267–275. [CrossRef] [PubMed]
36. Wang, D.P.; Zhao, Z.H.; Li, C.H. Universal Self-Healing Poly(dimethylsiloxane) Polymer Crosslinked Predominantly by Physical Entanglements. *ACS Appl. Mater. Interfaces* **2021**, *13*, 31129–31139. [CrossRef]
37. *ASTM-D7173*; Standard practice for determining the separation tendency of polymer from polymer-modified asphalt. ASTM International: West Conshohocken, PA, USA, 2020.
38. Yu, H.; Mo, L.; Zhang, Y.; Qi, C.; Wang, Y.; Li, X. Laboratory Investigation of Storage Stability and Aging Resistance of Slightly SBS-Modified Bitumen Binders. *Materials* **2023**, *16*, 2564. [CrossRef]
39. Yang, S.; Ji, J.; Tao, H.; Muhammad, Y.; Huang, J.; Wang, S.; Wei, Y.; Li, J. Fabrication of urea formaldehyde–epoxy resin microcapsules for the preparation of high self-healing ability containing SBS modified asphalt. *Polym. Compos.* **2021**, *42*, 4128–4137. [CrossRef]
40. *AASHTO T240*; Standard Method of Test for Effect of Heat and Air on a Moving Film of Asphalt Binder (Rolling Thin-Film Oven Test). AASHTO: Washington, DC, USA, 2023.
41. *AASHTO R28-12*; Accelerated Aging of Asphalt Binder Using a Pressurized Aging Vessel (PAV). AASHTO: Washington, DC, USA, 2015.
42. *AASHTO T48-06*; Standard Method of Test for Flash and Fire Points by Cleveland Open Cup. AASHTO: Washington, DC, USA, 2015.
43. *AASHTO T316*; Standard Method of Test for Viscosity Determination of Asphalt Binder Using Rotational Viscometer. AASHTO: Washington, DC, USA, 2022.
44. *AASHTO T315-20*; Standard Method of Test for Determining the Rheological Properties of Asphalt Binder Using a Dynamic Shear Rheometer (DSR). AASHTO: Washington, DC, USA, 2020.
45. *AASHTO T313-12*; Standard Method of Test for Determining the Flexural Creep Stiffness of Asphalt Binder Using the Bending Beam Rheometer (BBR). AASHTO: Washington, DC, USA, 2015.
46. *AASHTO M320-10*; Standard Specification for Performance-Graded Asphalt Binder. AASHTO: Washington, DC, USA, 2015.
47. Aurilio, R.M.; Aurilio, M.; Baaj, H. The effect of a chemical warm mix additive on the self-healing capability of bitumen. *J. Test. Eval.* **2022**, *50*, 1775–1782. [CrossRef]
48. Xie, W.; Castorena, C.; Wang, C.; Kim, Y.R. A framework to characterize the healing potential of asphalt binder using the linear amplitude sweep test. *Constr. Build. Mater.* **2017**, *154*, 771–779. [CrossRef]
49. Chen, H.; Bahia, H.U. Modelling effects of aging on asphalt binder fatigue using complex modulus and the LAS test. *Int. J. Fatigue* **2021**, *146*, 106150. [CrossRef]

Disclaimer/Publisher's Note: The statements, opinions and data contained in all publications are solely those of the individual author(s) and contributor(s) and not of MDPI and/or the editor(s). MDPI and/or the editor(s) disclaim responsibility for any injury to people or property resulting from any ideas, methods, instructions or products referred to in the content.